THE RATE-LIMITING STEP

IN

A GLUCOSE/OXYGEN BIOFUEL CELL

THE RATE-LIMITING STEP

IN

A GLUCOSE/OXYGEN BIOFUEL CELL

By

MINXUE ZHI, B.ENG., M. A. Sc.

A Thesis

Submitted to the School of Graduate Studies

In Partial Fulfillment of the Requirements

For the Degree

Master of Applied Science

McMaster University

MASTER OF APPLIED SCIENCE (2006) McMaster University

(Materials Science and Engineering) Hamilton, Ontario

TITLE: The Rate-limiting Step in a Glucose/Oxygen Biofuel cell

AUTHOR: Minxue Zhi, B. Eng. (Xi'an Jiaotong University)

M.A.Sc (Beijing Institute of Aeronautical Materials)

SUPERVISOR: Professor Gu Xu

NUMBER OF PAGES: XII, 87

Abstract

In this thesis, the rate-limiting step is determined in a biofuel cell with a bio-anode, a Nafion membrane and a conventional, platinum-based cathode using reference electrode method. It was discovered by surprise that the cathode overpotential dominated the cell overpotential. Na^+ in the membrane was found to hinder the H^+ transport. The cathode overpotential increased due to the presence of Na^+ in the membrane and at the cathode. The limited H^+ transport causes the increase of the cathode overpotential. H^+ transport is the rate-limiting step in our biofuel cell, rather than commonly believed electron transport. Moreover, the cell power output degradation is not due to the conventionally believed depletion of the fuel substrate, inter-penetration of the fuel and oxidizer and the degradation of the biocatalysts, but the limited H^+ transport in our biofuel cell.

The existing oxygen reduction mechanism at the cathode was questioned and revised. When Na^+ occupies all sulfonate groups in the membrane, only the Na^+ from the buffer can pass through the membrane. The oxygen reacts with the water transported with Na^+ and electrons to produce OH^-, which balances with the transported Na^+ to keep electroneutrality at the cathode.

Tris buffer without Na^+ was utilized as alternative anolyte in the biofuel cell. It was found that the cell with Tris buffer had a poorer performance in comparison with sodium phosphate buffer due to the increases of the anode and cathode overpotentials. Tris buffer does not constitute a solution to the problem.

This work represents a step toward a more complete understanding of the properties of biofuel cells. To improve biofuel cell output, the herein identified H^+ transport limitation in Na^+ contained Nafion needs to be overcome.

Acknowledgements

The author wishes to be deeply grateful to his supervisor, Dr. Gu Xu, for his patient and instructive supervision throughout the thesis work.

The author would like to thank Dr. Orville Hileman for his instructive discussion and advice.

Very special thanks must be given to Xiaohua Deng, Boris Martin, Dr. Nanda Nagarajan, Dr.Naveen Kumar and Jennifer Boyd for their invaluable discussion and great help.

The author would like to thank his group members, Dr. Huazhong Shi, Hualong Pan, Roy Luo, Richard Klenkler, and Feihong Nan, for their helpful advice and assistance with this project.

The author wishes to thank his wife, Jing Xu, for her constant support and encouragement.

The financial support from MMO and McMaster University is greatly appreciated.

Table of Contents

List of Figures

List of Tables

Chapter 1 Fundamentals of Biofuel Cells

1.1 What is a Biofuel Cell?

A biological fuel cell, abbreviated as biofuel cell, is an electrochemical device that uses biocatalysts for the conversion of chemical energy directly to electrical energy. It is a genuine fuel cell that holds promise in the long term (Shukla et al., 2004).

Unlike conventional fuel cells, biofuel cells operate under mild reaction conditions, namely ambient operation temperature and pressure. They can use a much wider ranger of renewable carbohydrates, such as sugars and alcohols, as fuels. Another distinctive feature of biofuel cells is that they utilize renewable biocatalysts, microorganisms or enzymes, as catalysts.

Biofuel cells have traditionally been classified into two types: microbial fuel cells and enzymatic fuel cells, named after their respective catalytic source, microorganisms or enzymes.

1.2 History of Biofuel Cells

Biofuel cells have a long history in literature. The first experiments in the field of biofuel cells were performed by M.C. Potter, a professor of botany, in 1910 (Shukla et al., 2004). He first demonstrated that E.coli could generate a voltage and deliver a current. These results were not widely reported until the experiments of Cohen in 1931 who achieved a voltage greater than 35 V from microbial fuel cells connected in electrical series.

Biofuel cells gained popularity in the 1960s, when NASA evinced interest in the development of microbial biofuel cells as a possible technology for a waste disposal

system for space flights that would also generate power. The first enzymatic biofuel cell was reported in 1964 using glucose oxidase (GOx) as anodic catalyst and glucose as fuel (Kim et al., 2006). Biofuel cells were already commercially available at that time, and they were promoted as power sources for radios, signal lights and other applications at sea. However, these fuel cells were not a commercial success and they soon disappeared from the market, due to the successful development of technology alternatives, such as photovoltaics.

During the oil crisis of the 70s and 80s, the interest in the development of biofuel cells was revived. Noteworthy are the contributions of Bennetto and co-workers (Shukla et al., 2004). They developed and demonstrated improved biofuel cells using various microorganisms and mediator systems. Mediators are low molecular weight redox species, which can assist the shuttling of electrons between bacteria or enzymes and an electrode. They showed that mediators could enhance the efficiency of electron transfer and reaction rate. After that, due to the wide application of mediators, the output power density of biofuel cells was improved remarkably. It was soon realized that biofuel cells would provide opportunities for practical applications. Thus, increasing effort has been placed on the research and development of biofuel cells since the 1990s.

1.3 Basic Principle of Biofuel Cells

Figure 1.1 shows the operational principle of an enzymatic fuel cell. In the anode compartment, one kind of enzyme (E1), such as glucose oxidase (GOx), is used as the biocatalyst. Glucose (fuel) is fed to anodic cell. The bio-catalytic half reaction in the anode side can be summarized as:

$$2\beta - D - glucose \rightarrow 2\delta - gluconolactone + 4e^{-} + 4H^{+} \qquad (1.1)$$

The electrons are transferred to the anode and protons flow through a proton exchange membrane (PEM) to the cathode. In order to increase the electron transfer efficiency, an electron transfer mediator (M1) is needed in the anode chamber. At the cathode, an electron acceptor is chemically reduced. Ideally, oxygen is used to accept the electrons and reduced by another kind of enzyme (Ė2), such as laccase, to water. Similarly, another electron transfer mediator (M2) is needed in the cathode side. The half reaction at the cathode can be summarized as:

$$O_2 + 4H^+ + 4e^- \rightarrow 2H_2O \tag{1.2}$$

The whole cell reaction thus is:

$$2\beta - D - glucose + O_2 \rightarrow 2\delta - gluconolactone + 2H_2O \tag{1.3}$$

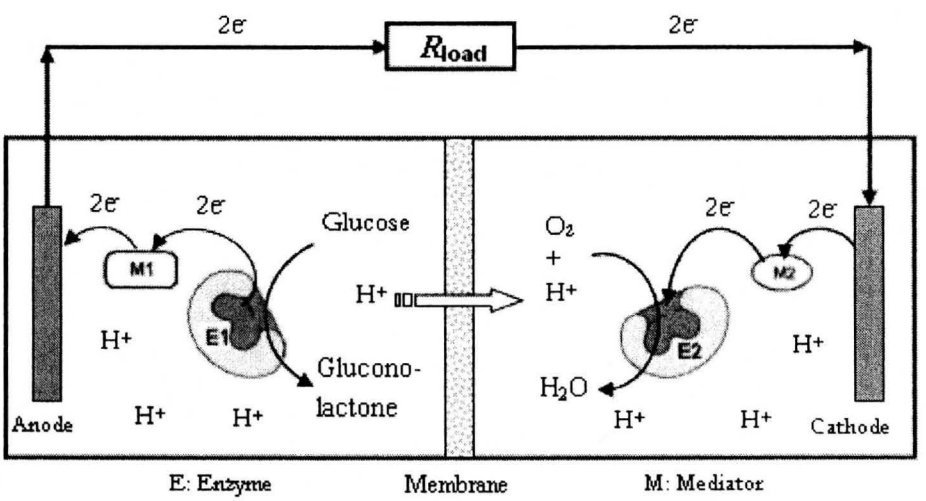

Figure1.1 The working principle of an enzymatic fuel cell

Clearly, for both these reactions to proceed continuously, electrons produced at the anode compartment must pass through E1 to M1 to anode, and through an electrical circuit to the cathode, then through M2 to E2. Also, H^+ must pass through the PEM. In this way, the chemical energy is transformed to electric energy.

Microbial fuel cells work in a similar way to enzymatic fuel cells. The main difference is that microorganisms are utilized as biocatalysts in microbial fuel cells.

1.4 Microbial Fuel Cells

Microbial fuel cells were the earliest biofuel cell technology to be developed. They can operate on variable fuels, and are usually capable of oxidizing the substrate completely to carbon dioxide and water. Microorganisms can be used in four ways for producing electricity (Vielstich et al., 2003; Shukla et al., 2004):

1) Microbial-system producing hydrogen as fuel for conventional fuel cells

Hydrogen is produced in a separate bioreactor through microbiological fermentation process and transported to the anode of a conventional fuel cell (generally high temperature Solid Oxide Fuel Cell (SOFC)) to convert this biofuel gas into electricity. The most effective hydrogen-producing microorganism is C.butyricum. One of the major drawbacks of this configuration is the low efficiencies of biological substrate to hydrogen conversion and the requirement of high fuel cell temperatures to obtain sufficient hydrogen oxidation. Moreover, the produced biofuel gas is not sufficiently pure for direct use in fuel cells, due to contamination caused by CO, H_2S and (poly) siloxanes.

2) The integrated bioreactor microbial biofuel cells

In this configuration, the fermentation process is conducted directly in the fuel cell itself by supplying the anode with H_2 fuel. In addition to H_2, the by-products, formic acid, lactic acid and S^{2-} species may be produced during the fermentation. Formic acid and lactic acid can be used as fuels. However, the presence of sulphides in the medium

results in the inhabitation of metabolic bacterial processes because of their interaction with iron-containing protein. Moreover, S^{2-} species poison many metallic electrodes because of their strong irreversible adsorption, which leads to poor biofuel cell performance.

3) The microbial biofuel cells with mediated electron transfer

The direct and efficient electrical communication between microorganisms and electrodes are usually hindered by microbial membranes except in some special cases described later. The cells can, however, be wired to the electrode surface with the help of mediators. Thionine and organic dyes have been frequently used as mediators in microbial biofuel cells. The overall efficiency of electron transfer mediators depends on many parameters, particularly on the electrochemical rate-constant of mediator re-oxidation. It is difficult to realize the perfect conditions for electron transfer from a bacterial cell to an electrode. A mixture of two mediators can be useful in optimizing efficiency.

The mediators can be coupled to the microorganisms in three ways: a) as diffusional mediators shuttling between the microbial suspension and the anode surface; b) diffusional mediators shuttling between the anode and microbial cells covalently linked to the electrode; c) mediators absorbed on the microbial cells.

4) The microbial biofuel cell with direct electron transfer

Metal-reducing bacteria are the most used species in this configuration. They can directly transfer electrons on the electrode as they have cytochromes in their outer membranes. Mediator-less microbial biofuel cells have an advantage over those with mediators in terms of cost as well as non-desirability of toxic mediators. Fuels that can be used in this configuration are limited to simple organic acids, such as acetate. Recently, it was observed that R.ferrireducens, a dissimilatory Fe(III)-reducing microorganism, could completely oxidize sugars coupled to Fe(III) reduction(Chaudhuri and Lovely, 2003).

1.5 Enzymatic Fuel Cells

A microorganism is a multi-enzyme system. It is enzymes that work as the biocatalysts in microbial biofuel cells. The enzymes responsible for the desired process can be separated and purified from living organisms, and applied as biocatalysts in biofuel cells rather than using the whole microbe cells. Unfortunately, there are three critical issues with the application of enzymes in biofuel cells: enzyme activity, stability and electron transfer between enzymes and the electrode surface.

1.5.1 Effects of Temperature and pH Value on Enzyme Activity

Enzymes are bio-catalysts, which are sensitive to pH value and temperature changes (Figure 1.2 and 1.3, data from Roche Applied Science). As far as GOx is concerned, the optimum pH value and temperature are pH 7 and 25°C, respectively. Enzymes work well at room temperature. To keep a constant pH value, buffer solutions are generally used in biofuel cells (Rozendal et al, 2006; Gil et al, 2003; Mano et al, 2003).

1.5.2 Enzyme Stability

In most cases, the stability of the enzymes themselves determines the lifetime of biofuel cells. It is self-evident that pH value and temperature will affect enzyme stability. The application configuration of enzyme plays a more important role in biofuel cells. Soluble hydrogenase loses its activity after 2 days, while immobilized hydrogenase preserves 50% of its initial activity even after half a year (Figure 1.4). Enzyme immobilization improves enzyme stability, which can be achieved either chemically or physically (Kim et al., 2006).

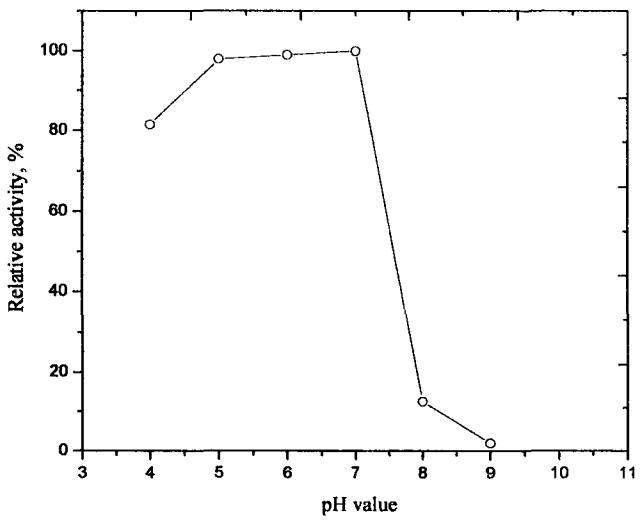

Figure 1.2 Effects of pH value on GOx activity

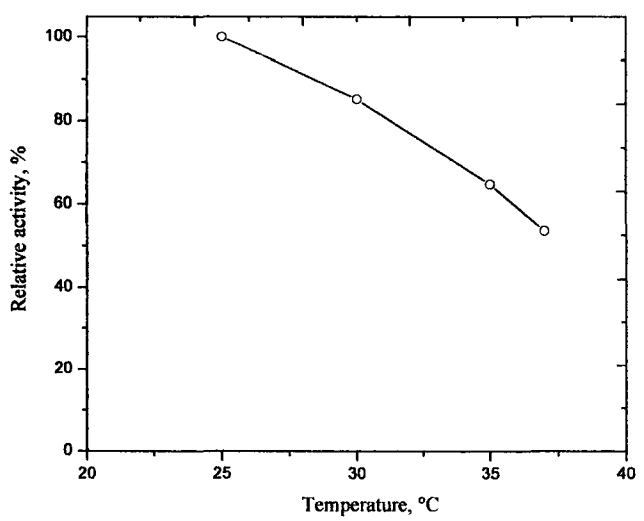

Figure 1.3 Effects of temperature on GOx activity

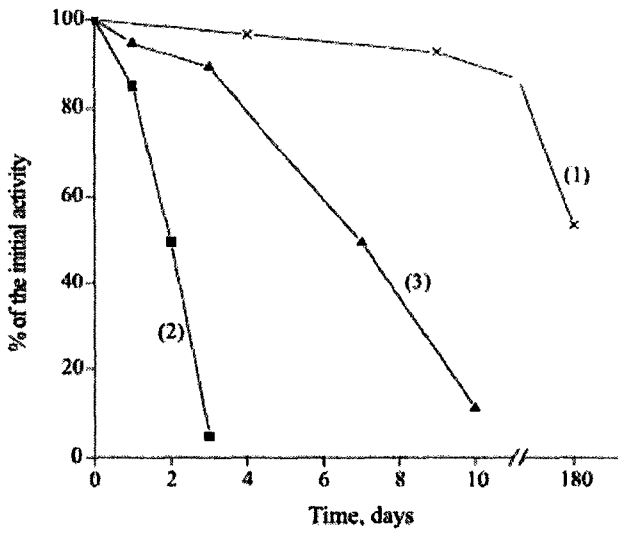

Figure 1.4 Hydrogenase stability: (1) immobilized on carbon filament material electrode (2) soluble (3) soluble with stabilizer (Karyakin et al., 2002)

1.5.3 Electron Transfer in Enzymatic Fuel Cells

Enzymes have a complex structure comprised of proteins. The electron-transferring unit of enzymes, the active centre, is surrounded by its protein matrices. Hence, efficient electrical communication between electrode and enzymes is difficult.

Enzymes can be divided into three groups when discussing methods of establishing electron transfer between enzymes and electrode (Figure 1.5).

The first group has enzymes with Nicotinamide Adenine Dinucleotide ($NADH/NAD^+$) or Nicotinamide Adenine Dinucleotide Phosphate ($NADPH/NADP^+$) redox centres (e.g. lactate dehydrogenase), which are often weakly bound to the protein of the enzyme. The active centre can diffuse out of the enzyme and travel to the electrode, transferring electrons itself. In a biofuel cell, this allows the cofactor to also function as a natural redox mediator.

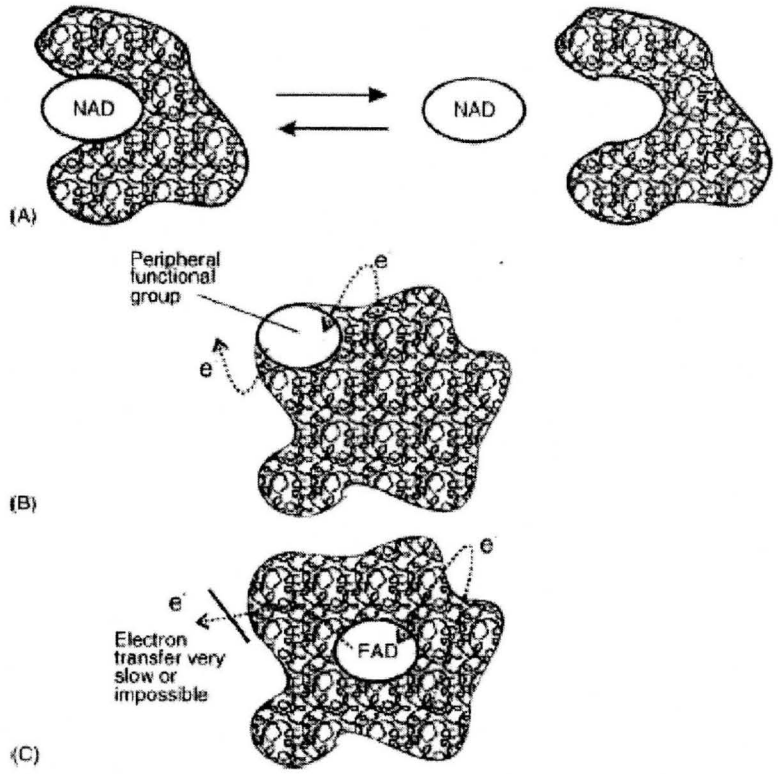

Figure 1.5 The different locations of enzyme active centres and how they affect electron transfer in unmodified enzymes. (A) Enzyme active centre is NAD(H) or NADP(H). (B) The active centre is located on the periphery of the enzyme. (C) The enzyme has strongly bound redox centres, surrounded by the glycoprotein shell (Bullen et al., 2006).

In the second group of enzymes at least part of the redox centre is conveniently located at or near the periphery of the protein shell (e.g. peroxidases). The active centre (often porphyrin derivatives) is located on the periphery of the enzyme, and can transfer electrons directly to (or receive electrons from) an electrode.

The third type of enzyme has a strongly bound redox centre (e.g. Flavin Adenine Dinucleotide (FAD)), which is deeply bound in a protein or glycoprotein shell. Direct electron transfer from the active centre is either extremely slow or impossible, requiring the use of mediator molecules capable of penetrating into the enzyme to transport charge.

GOx is the most studied this type of enzyme for biosensors and biofuel cells.

In general, electron transfer between enzyme and electrode is classified by two different mechanisms (Figure 1.6): direct electron transfer (DET) and mediated electron transfer (MET). Depending on the enzyme and reaction conditions, rates of MET can exceed by orders of magnitude those of DET (Barton et al., 2004)

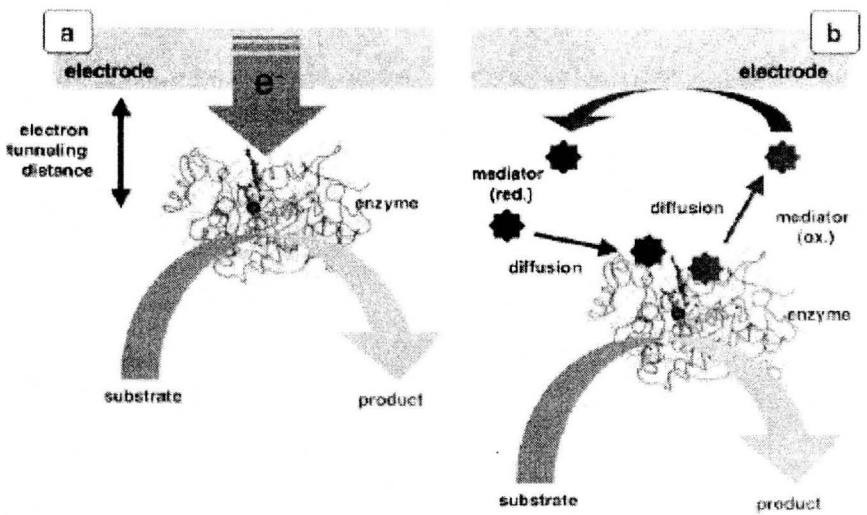

Figure 1.6 (a) Direct electron transfer from electrode surface to the active site of an enzyme. (b) Electron transfer via redox mediator (Barton et al., 2004)

Corresponding to the two electron transfer mechanisms, two different kinds of enzymatic electrodes have been developed for enzymatic fuel cells (Bullen et al., 2006):

1. Non-diffusive enzyme electrodes. For some enzymes with peripheral redox centres, DET can be achieved by contacting with the electrode without a mediator. For other enzymes with strongly bound redox centres, the techniques used to establish direct and efficient electrical communication between enzymes and electrodes have evolved from attempting connection by simple adsorption, through entrapment in conductive polymers, to methods connecting the active centre either through a defined structured

path or a highly conductive redox group-modified polymer electrostatically retaining the enzyme, and latterly with partially mobile redox groups able to penetrate to the active centre (Bullen et al., 2006).Those enzyme immobilization methods not only improve the electron transfer between enzymes and electrode surface, but also enzyme stability.

2. Diffusive MET enzymatic electrodes. This class of enzymatic biofuel cell system involves weakly bound NADH or NADPH active centres diffusing to the electrode, and an artificial mediator molecule shuttling between the enzyme with strongly bound redox centres and the electrode. The mediator is regenerated at the electrode surface and circulates continuously between the enzyme and the electrode. Since the driving force for electron transfer is potential difference, the choice of appropriate mediators is limited to those with redox potentials close to that of the chosen enzyme. The electrode provides a boundary condition for electron flux to and from solution. As shown in Figure 1.7, the open-circuit potential of a glucose-oxygen biofuel cell is primarily determined by the difference in redox potential of the two mediator couples.

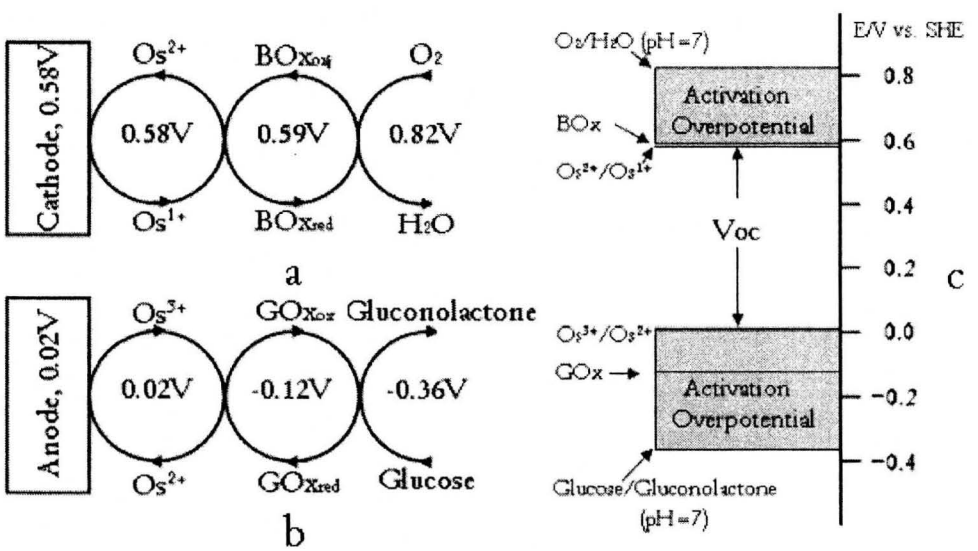

Figure 1.7 Potential schematic for a mediated biofuel cell (Barton et al., 2004)

1.5.4 Enzymes and Mediators Used in Enzymatic Fuel Cells

Enzymes and mediators, which can be utilized in an enzymatic fuel cell, were summarized by Liu et al. (2005). GOx, glucose dehydrogenase, lactate dehydrogenase, and alcohol dehydrogenase can be used as the anodic biocatalysts, whereas microperioxidase-11, cytochrome oxidase (COx), bilirubin oxidase (BOx), and laccase are often adopted as the cathodic catalysts. Due to their plentiful sources and good catalytic properties, GOx and laccase have been cooperatively assembled into biofuel cells. Mediators often adopted for GOx include polymer-Os, pyrroloquinoline quinone (PQQ), ferrocene (Fc) and its derivatives, ferricyanide, methylene blue, benzoquinone, and N-methyl phenazine. At present, PQQ is considered to be the best mediator for GOx due to its formal potential being relatively low. Unfortunately, the high costs involved limit its application. In comparison, the stable and low-cost Fc has been used as mediator for the anode of an enzymatic biofuel cells. Common mediators of laccase include 2, 2'-azinobis (3-ethylbenzthiazoline-6-sulfonic acid) diammonium salt (ABTS), syringal dazine, Fc, $K_3Fe(CN)_6/K_4Fe(CN)_6$, I_2/I_3^-, and polymer-Os. ABTS was found to be the best electron mediator for use in the cathode of enzymatic biofuel cells, because it exhibits a relatively high formal potential, and is easily obtainable.

1.6 Comparison of Microbial and Enzymatic Fuel Cells

By tapping the complete multi-enzyme metabolic pathways inside living cells, microbial fuel cells exhibit unique features unmatched by enzymatic fuel cells, such as long-term stability, complex fuels and fuel efficiency. However, the power densities associated with microbial fuel cells are typically much lower owing to resistance to mass transfer across cell membranes. Enzymatic fuel cells demonstrate reduced stability because of the limited lifetime of extracellular enzymes and are unable to fully oxidize fuels. However, enzymatic fuel cells are compatible with immobilization and wiring, and,

consequently, can offer high power densities, especially when used in concentrated form.

1.7 Applications of Biofuel Cells

Biofuel cells copy nature's solutions to energy generation. They consume renewable biomass. The energy liberated during the complete oxidation of glucose to CO_2 and water is about 16×10^6 J/kg, which is about 5 kWh of electrical energy. A medium-sized car that needs about 200 Wh/km could travel 25-30 km on 1 kg of a strong sugar solution in theory (Shukla et al., 2004).

An intuitive application of biofuel cells is used as implantable power for medical devices, such as pacemakers and drug delivery devices. Biocatalysts are physiological species, efficiently catalyzing reactions at physiological temperature and pH. Moreover, the medical devices can utilize glucose, a sugar present in the blood system, as fuel, and can draw power as long as the subject lives. A biofuel cell that is just 0.07 cm^2 in area has been designed to generate as much as 300 μV for 2 h, an amount sufficient to operate tiny devices, including microscopic drug-delivery systems (Figure 1.8(a)) (Haselkorn 2002).

Biofuel cells can also be utilized in the field of waste water engineering. It is known microorganisms can be used to generate electricity. When they oxidize organic compounds in waste water, electrons are released yielding a current. An experiment by Penn State environmental engineers produced a power density of 26 mW/m^2, while removing up to 80% of chemical oxygen demand (COD) of the waste water (Liu et al., 2004). If power generation in these systems can be increased, microbial biofuel cell technology may provide a new method to offset wastewater treatment plant operating costs.

One more interesting application is a robot powered by a biofuel cell (Wilkinson 2000). The "Gastrobot", uses a microbial fuel cell system to directly convert carbohydrate

fuel to an electrical power source without combustion (Figure 1.8(b)). Gastrobot is thought to be the first robot of its kind to use such a novel biomass energy conversion method, and as such represents a new class of bioelectromechanical machines. Gastrobot can potentially be sustained from just an input of natural food, water and air, and is therefore ideal for a host of applications that demand "living off the land" during fully autonomous "start and forget" missions.

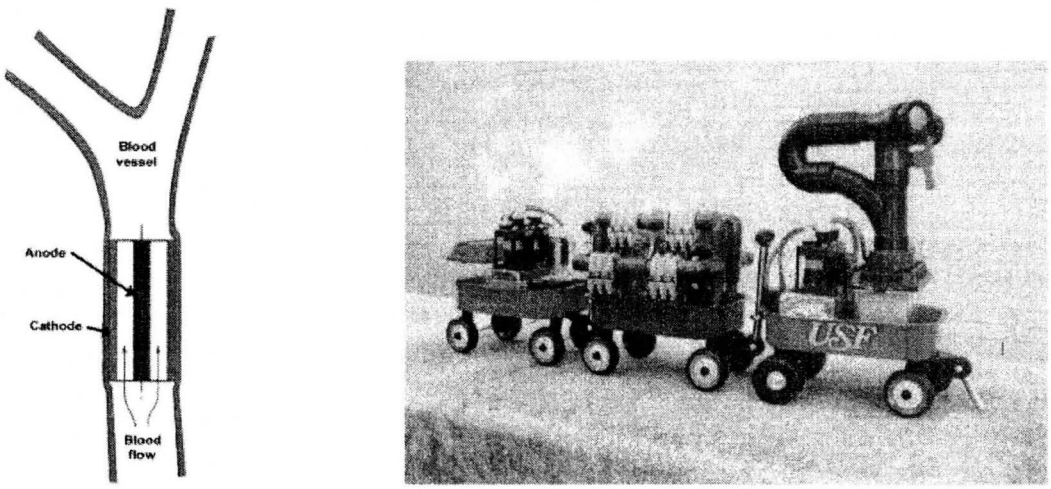

(a) (b)

Figure 1.8 Applications of biofuel cells. (a) A biofuel cell directly attached to the blood vessel (Haselkorn 2002) (b) "Gastronome"—a prototype microbial fuel cell powered robot (Wilkinson 2000).

1.8 Problem Statement & Research Objectives

Biofuel cells have been studied for nearly a century, but they have not advanced to the point of practical use at present. The performance of biofuel cells, in terms of power density, lifetime and operational stability, falls far below that of chemical fuel cells

(Kim et al., 2006). The low current density is a primary challenge for the application of biofuel cells. Platinum-based hydrogen-air fuel cell electrodes typically operate nearly 1 A/cm^2 and 0.65 V and methanol cells achieve 0.5 A/cm^2 at 0.5 V, orders of magnitude higher than the 1～10 mA/cm^2 current densities obtainable using the best reported methanol-air biofuel cells to date (Barton et al., 2004).

If biofuel cells are to find a practical application there is a credibility gap (Figure 1.9) that must be bridged. Many applications for biofuel cells require a power output in the range of 10～100 mW/cm^2. To construct biofuel cells with high power densities, the detailed characterization of the interfacial electron transfer rates, biocatalytic rate-constants and cell resistance is essential. Identification of the rate-limiting steps allows the development of strategies to improve and enhance the cell output.

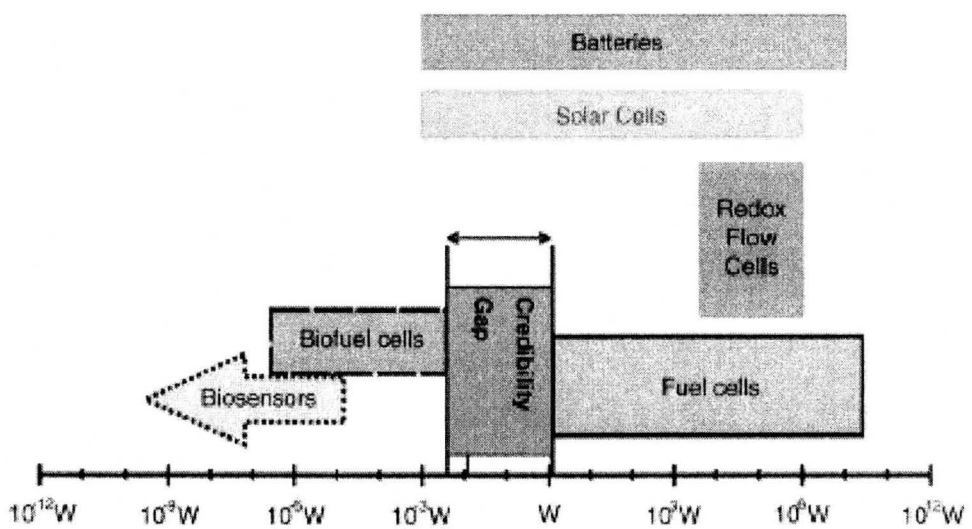

Figure 1.9 Approximate power output ranges of biosensors, biofuel cells and inorganic fuel cells, illustrating the scale of the credibility gap challenging the biofuel cell researchers (Bullen et al., 2006).

Therefore, the objective of my research is to determine the rate-limiting step in biofuel cells, including the following points:

a) Survey all possible rate-limiting steps in biofuel cells;

b) Determine the rate-limiting step in biofuel cells by reference electrode and electrochemical impedance spectroscope methods;

c) Investigate the reasons for the increase of electrode overpotential;

d) Based on our results, build a new understanding of the performance limiting factors in biofuel cells.

Because enzymatic fuel cells can offer high power densities, and have good future prospects, our research will focus on this kind of biofuel cells.

1.9 Thesis Overview

The thesis consists of five chapters. Chapter 1 provides the fundamentals of biofuel cells, including the definition, classification, working principle, potential applications and problems of biofuel cells. Chapter 2 involves literature review, including possible rate-limiting steps and methods to determine rate-limiting step in biofuel cells. Chapter 3 details the experimental methods and instruments. Chapter 4 provides the experimental results, analysis and discussion. Chapter 5 presents the conclusions.

Chapter 2 Literature Review

Extensive literature review exists in the area of biological fuel cells. Notably, Palmore and Whitesides (1994) summarized biological fuel cell concepts and performance up to 1992. More recently, Katz and Willner (2003) discussed recent progress in novel electrode chemistries for both microbial and enzymatic fuel cells, and Heller (2004) reviewed advances in miniature cells. Barton et al. (2004) analyzed the strengths and weaknesses of the technology in the context of specific classes of applications and pointed out areas where additional knowledge is required to properly exploit enzymatic fuel cells. Bullen et al. (2006) critically reviewed the performance and carefully analyzed the current direction of development of biofuel cells. In this chapter, a literature review related to rate-limiting steps in biofuel cells will be presented.

2.1 Description of Electrochemical Processes in Biofuel Cells

Consider the biofuel cell shown in Figure 1.1: the question arises how we can further understand the electrochemical processes happening in biofuel cells. Generally, there are four levels that describe the cell reaction processes of fuel cells: electrochemistry, thermodynamics, steady state kinetics, and transient behavior.

2.1.1 Electrochemistry

Electrochemistry studies the reactions that take place at the interface of an electronic conductor and an ionic conductor. Returning to the enzymatic fuel cell in Figure 1.1, with an open circuit, no current is flowing, and the partial reactions occurring at the anode and cathode are at equilibrium. By definition, equilibrium exists when the chemical potential of the products equals that of the reactants, so

$$2\mu^a(\beta-D-glucose) = 2\mu^a(\delta-gluconolactone) + 4\mu^a(H^+) + 4\mu^a(e^-) \quad (2.1)$$

and

$$\mu^c(O_2) + 4\mu^c(H^+) + 4\mu^c(e^-) = 2\mu^c(H_2O) \quad (2.2)$$

where μ^a and μ^c refer to the chemical potentials at the anode and cathode, respectively. Since the H^+ can be assumed to migrate freely through the electrolyte, the chemical potentials of H^+ at the two electrodes are also at equilibrium:

$$\mu^a(H^+) = \mu^c(H^+) \quad (2.3)$$

The voltage difference that appears between anode and cathode simply reflects their different electrochemical potentials:

$$E_r = \frac{\mu^c(e^-) - \mu^a(e^-)}{q_e}$$

$$= \frac{2\mu^a(\delta-gluconolactone) + 2\mu^c(H_2O) - 2\mu^a(\beta-D-glucose) - \mu^c(O_2)}{4q_e}$$

$$= \frac{\Delta G}{4q_e} \quad (2.4)$$

where $-q_e$ is the electron's charge, and ΔG is the change in Gibbs free energy for the reaction Eq.1.3.

From electrochemistry, we learn that an electrical potential appears between the electrodes because of the excess of electrons at the anode compared with the cathode. It is this potential difference that drives current through the external load, making the fuel cell a source of power.

2.1.2 Thermodynamics

For the reversible electrochemical reaction Eq.1.3, the theoretical maximum available work is given by

$$W = nFE_r = -\Delta H - Q = -(\Delta H - T\Delta S) = -\Delta G \quad (2.5)$$

where n is the number of electrons transferred per mole of reactants, F is the Faraday constant, E_r is the electromotive force (EMF) of the cell reaction, ΔH is the enthalpy change, or the energy released by the reaction, and Q is the heat generated by the reaction.

From equation 2.5, we can derive the EMF of the cell by

$$E_r = -\Delta G/nF \quad (2.6)$$

There are thermodynamic data available in the literature to calculate the change in Gibbs free energy for reactions. Some are listed in Table 2.1. Thus, for the cell reaction in Figure 1.1 at 25°C, pH 7, 0.1 M ionic strength, and O_2 at 1atm, according to Eq. (2.6) the EMF of the fuel cell is 1.18 V.

Table 2.1 Standard transformed Gibbs energies of formation $\Delta_f G°$ of biochemical reactants at 25°C, pH 7, and three ionic strengths (Alberty, 2000)

	$\Delta_f G°$/kJ mol^{-1}		
Ionic strength/M	0	0.10	0.25
β -D-Glucose(aq)	-436.42	-429.08	-426.71
δ -Gluconolactone(aq)	-506.38	-500.26	-498.28
H_2O(aq)	-157.28	-156.05	-155.66
O_2(g)	0	0	0

2.1.3 Steady State Kinetics

Fuel cells operate under thermodynamically irreversible conditions. The greater the current density provided by a fuel cell, the further it must be perturbed from equilibrium, and the further the operating voltage will sink below the ideal theoretical voltage. These irreversibilities are separately categorized as activation, ohmic and concentration losses. Activation losses (η_{act}) are associated with overcoming reaction energy barriers at the electrode–electrolyte interfaces. Ohmic losses (η_{ohm}) are associated with electron and ion conduction processes occurring in the electrodes, electrolyte, and interconnects, as well as the contact resistances across each material interface. Concentration losses (η_{conc}) are associated with reactant and product diffusion limitations between the bulk flow and reaction sites. These losses coexist, but each dominates different regions. A typical relationship between voltage and current density, namely IV curve, is shown in Figure 2.1.

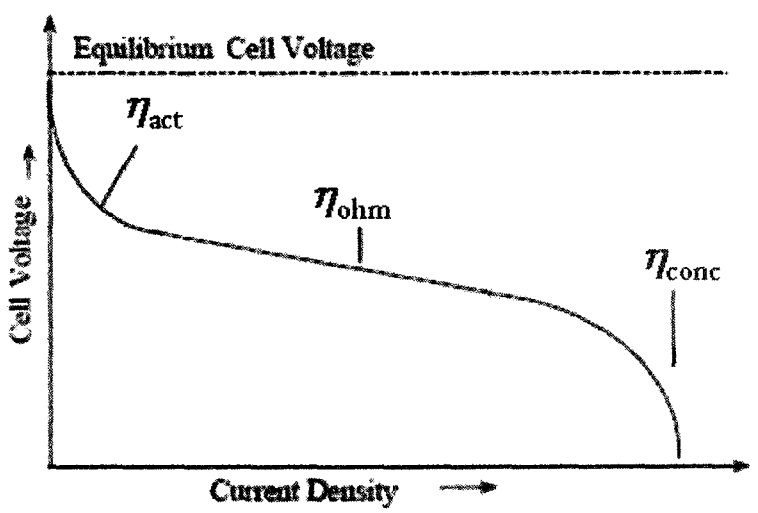

Figure 2.1 Schematic of a typical IV curve for fuel cells

All these irreversibilities can be brought together to construct an equation to model the performance of fuel cell performance (Zaluski, 1997):

$$E = E_r - (\eta_{act} + \eta_{ohm} + \eta_{conc})$$
$$= E_r - a\log i - d - bi + c\log\left(\frac{i_L - i}{i_L}\right) \quad (2.7)$$

where E is the operating voltage of fuel cell, a is Tafel slope, b is the cell internal resistance per unit cell area, c and d are constants, and i_L the maximum current attainable by the cell.

The IV curve of a glucose/O2 biofuel cell in Figure 2.2 shows the same shape as Figure 2.1.

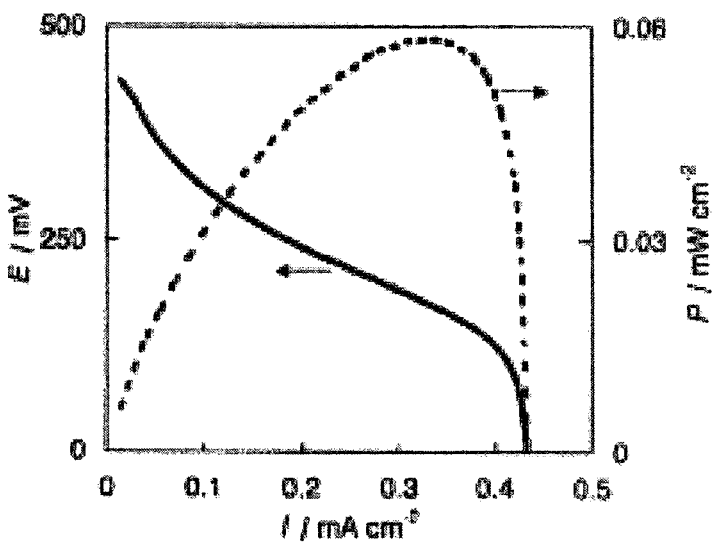

Figure 2.2 Performance of a glucose/O_2 biofeul cell (Tsujimura et al., 2002)

The IV curve is one method to characterize the performance of a fuel cell, which can be determined by either scanning the whole potential range continuously, from the open circuit potential to full load, with a constant voltage scan rate and recording the resulting current, or gradually altering the potential, and recording the steady state current after a definite time period (Barsoukov and Macdonald, 2005).

2.1.4 Transient Behavior

Thermodynamics characterizes equilibrium state, and kinetics characterizes steady state. The two states are all time-independent. Following this, we can ask how long it takes to change from the equilibrium state to the steady state and what occurs during this period? This involves the fourth level of description of fuel cells, transient behavior.

As far as a PEM fuel cell is concerned, three primary processes govern the time response (Wang, 2004). They are electrochemical double-layer discharging, gas transport through channel and gas diffusion layer (GDL), and membrane hydration or dehydration. The time constant of double-layer discharging is between micro- and milliseconds. The time constant for a reactant gas to transport through GDL can be estimated simply by its diffusion time. This gives a time constant between 0.1 and 1 s. The slowest process, however, is membrane hydration. For Nafion 112 and a reference current density of 1 A/cm^2, this is about 25 s.

The current interruption technique (CI) and electrochemical impedance spectroscopy (EIS) are two widely used methods to investigate the transient behavior of fuel cells (Jaouen et al., 2003)

2.2 Possible Rate-limiting Steps in Biofuel Cells

2.2.1 The Concept of a Rate-limiting Step

When a fuel cell works, it involves diverse and complex electrochemical and transport phenomena occurring at disparate length and time scales, such as fuel supply,

electron transport, ion transport and so on. However, a basic rule for a fuel cell working at steady state is that the current in the circuit is equal everywhere (Figure 2.3).

Rate-limiting step is often described as the slowest step in a pathway. At steady-state, all steps proceed at the same rate, determined by the rate-limiting step. Figure 2.4 illustrates a better description of a Rate-limiting Step.

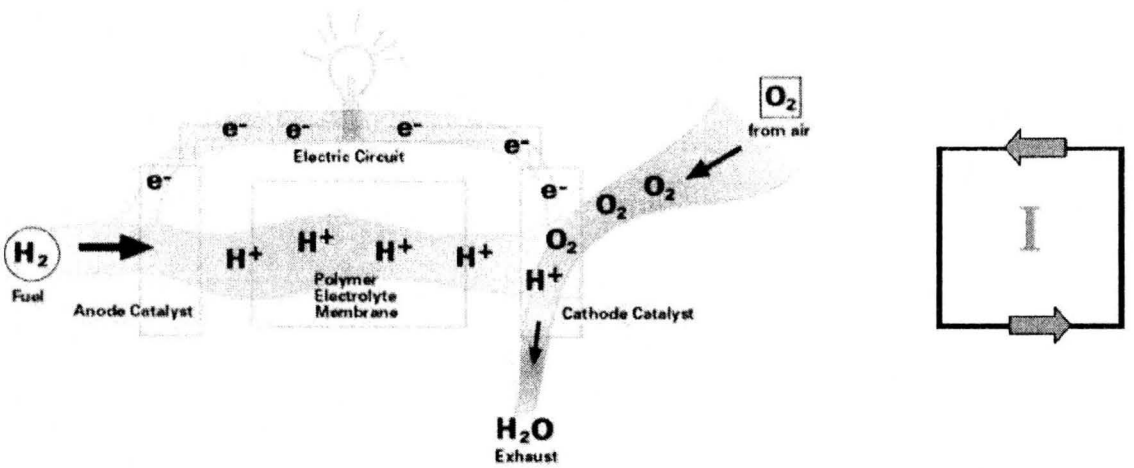

(a) (b)

Figure 2.3 (a) The pathway of a PEM fuel cell (www.vss.psu.edu) (b) The current is equal everywhere in the circuit at steady state.

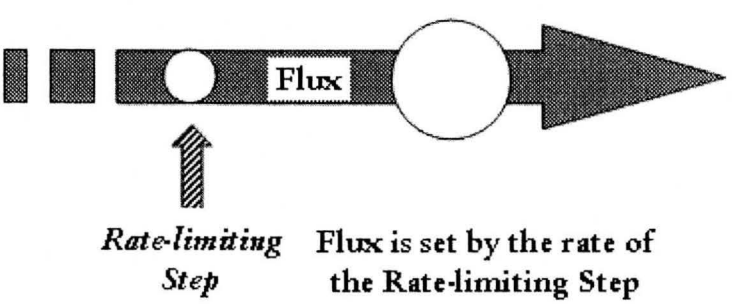

Figure 2.4 The rate-limiting step in a pathway.

To increase the power density of a biofuel cell, the rate-limiting step must be identified, and then improved. Only when the rate-limiting step is made more efficient can the power density of the fuel cell be increased.

The possible rate-limiting steps in an enzymatic fuel cell (Figure 1.1) can be generally categorized as a) enzyme catalytic rate; b) electron transport; c) proton transport; d) mass transport; e) internal resistance (Skukla et al., 2004). They are related to different overpotentials, respectively.

2.2.2 Enzyme Catalytic Rate

Enzymes are efficient catalysts. A measure of the enzyme catalytic rate is by specific activity U (1U≡1μmol of product produced per min at pH 7 & 25℃). Suppose the specific activity of GOx used in an enzymatic fuel cell in Fig. 1.1 is 1.65 U/mg (values of 0.1 to 10 U/mg are common), the current generated theoretically is 5.28 mA/mg (GOx), according to the cell reaction of equation 1.3.

By contrast, the state-of-the-art Pt-loading for H_2-fed anode electrodes is as low as 0.05 mg Pt/cm^2, while cathode loadings of 0.4 mg Pt/cm^2 are limited by the poor activity of Pt for the oxygen reduction reaction. The hydrogen-air fuel cell based on such Pt-loading operates around 1 A/cm^2 at 0.65 V (Gasteiger et al., 2004). Therefore, the state-of-the-art Pt mass activities are 2.5 A/mg (Pt) for O_2 and 20 A/mg (Pt) for H_2 at 0.65 V.

Another challenge is enzyme loading. As mentioned before, soluble enzymes have poor stability. Enzymes are generally immobilized on electrodes in biofuel cells. High enzyme loading is critical for high power density. When GOx is randomly packed as a monolayer on a flat electrode, the enzyme loading is only 1.7×10^{-12} mol/cm^2 (0.27 μg/cm^2), which was determined by the size of GOx. Assuming all the enzyme molecules are as active as in aqueous solutions with a typical turnover number of 600 s^{-1}, the upper

limit of the current density is about 0.2 mA/cm^2 (Kim et al., 2006). Therefore, multiple-layer enzyme assembly is needed to increase enzyme loading. Recently, Tamaki and Yamaguchi (2006) reported a 3-D electrode structure (Figure 2.5), with enzyme loading 10^4 times higher than that of a densely packed monolayer, and by which a 3 mA/cm^2 current at 0.6 V vs. Ag/AgCl was achieved.

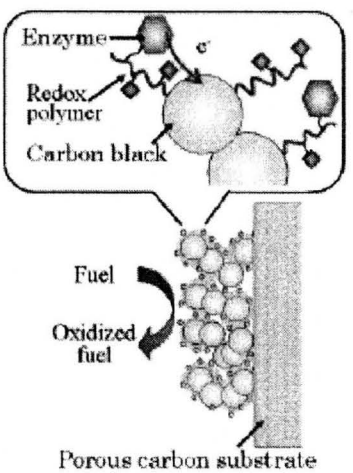

Figure 2.5 Schematic of a 3-D biofuel cell electrode (Tamaki and Yamaguchi, 2006).

Most enzymes are only moderately active. The uniqueness of enzymes lies in their selectivity and amenability to metabolic control, rather than in their ability to accelerate reactions. In terms of activity and stability, enzymes will find it difficult to surpass Pt and Pt-alloy chemical catalysts in PEM fuel cells (Palmore and Whitesides, 1994).

Catalysts are one of the key parameters to affect exchange current density of electrodes, which is a quantitative measure of the rate of reaction which occurs in opposite directions at equal rates at an interface at equilibrium. Due to the poor catalytic ability of enzymes compared with Pt and Pt-alloys, the exchange current density of

enzyme electrodes will be smaller than that of the Pt electrode. Furthermore, activation losses of fuel cells are dependent on the exchange current density according to Tafel equation (Larminie and Dicks, 2003). Theoretically, activation losses of biofuel cells will be larger than that of chemical fuel cells at the same current density.

2.2.3 Electron Transport

As mentioned before, direct electron transfer is in question for the enzymes with strongly bound redox centres. If one views the electrode and the enzyme redox center as a donor-acceptor pair, the thick protein layer surrounding the active center provides an effective kinetic barrier to electron-transfer. According to the Marcus electron transfer theory, the electron transfer rate decreases exponentially with this distance for electron transfer (Marcus, 1993):

$$k_{et} \propto \exp(-\beta(d - d_0)) \times [-(\Delta G_0 + \lambda)^2 / 4\lambda RT] \quad (2.8)$$

where k_{et} is the electron-transfer rate between a donor-acceptor pair, β is the rate of the decrease in electronic coupling with distance, d is the distance for electron transfer, d_0 is the van der Waals contact distance, ΔG_0 is the reaction energy (driving force), λ is the reorganization energy, and R and T are the gas constant and the temperature.

Therefore, the inefficient electron transfer between biocatalysts and electrodes was always thought as one of the critical challenges in developing biofuel cells (Persson et al., 1985; Kim et al., 2006; Palmore and Whitesides, 1994).

2.2.4 Proton Transport

2.2.4.1 Proton Transport at Transient and Thermodynamic Equilibrium States

Figure 2.6 schematically shows proton transport in a transient reaction process and in a thermodynamic equilibrium state at an open circuit in a PEM fuel cell. H_2 dissociates spontaneously into protons and electrons at the triple interfaces. Electrons are then transferred to carbon, and protons to Nafion, a proton exchange membrane. At the cathode, oxygen spontaneously dissociate into atoms, which combine with electrons and the migrating H^+ to produce water (Figure 2.6 (a)). Since the proton transport is from anode side to cathode side in Nafion, the reactions at the anode and cathode will continuously take place. As a result, an electric potential appears between the electrodes due to excess electrons at the anode (where they are generated) and deficient electrons at the cathode (where they are consumed). The transport of positive charged protons from the anode to the cathode is the prerequisite for the generation of electric potential between the electrodes. Therefore, if the proton pathway is blocked, a potential difference can not be achieved. When a thermodynamic equilibrium state is reached, the electrochemical potentials of H^+ at the two electrodes are equal in the equilibrium state, and H^+ migrates freely through the electrolyte (Figure 2.6 (b)).

A schematic diagram of the charge double layer in a PEM fuel cell is also shown in Figure 2.6(b). At the anode, H_2 dissociates spontaneously into protons and electrons, thereby leaving excess electrons in the anode, causing it to become negatively charged. Since the anode is negatively charged, there will be an electrostatic field in close proximity to the anode surface, causing the positively charged H^+ to be attracted to anode to form the charge double layer at the anode surface. Similarly, at the cathode, oxygen reacts with electrons from cathode and the migrating H^+ to form water. Since the electrons at the cathode are consumed, the cathode will be positively charged to cause negatively charged ions to be attracted to cathode to form the charge double layer at the cathode surface. Now the question is what is the identity of negative charged ions at the cathode surface?

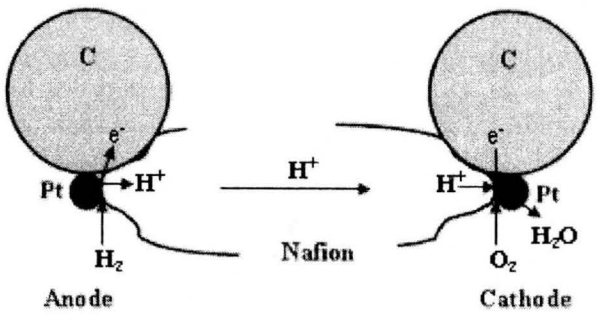

(a)

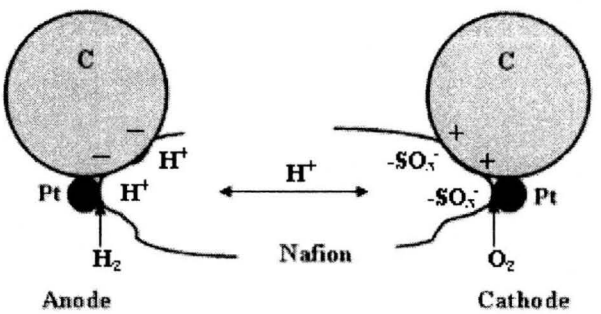

(b)

Figure 2.6 Proton transport (a) in a transient reaction process and (b) at an equilibrium state in a PEM fuel cell

Larminie and Dicks (2003) tried to describe the construction of the double layer at the surface of an acid electrolyte fuel cell cathode. Unfortunately, they only described the situation before the reaction happens at the cathode, which is not worth considering in practice.

Garcia (2001) proposed that the negatively charged ions were oxide ions (O_2^-) in the double layer at the cathode surface in a PEM fuel cell. However, it is well known the oxygen reduction reaction (ORR) mechanism is explained by bridge model (Yeager, 1984), illustrated in Figure 2.7. There are no oxide ions generated in oxygen reduction

reaction in a PEM fuel cell.

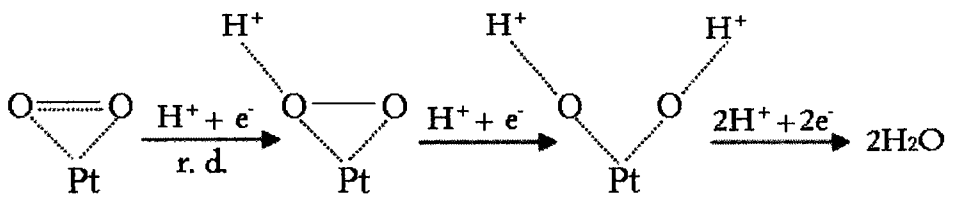

Figure 2.7 The bridge model of oxygen reduction on Pt (Yeager, 1984)

Recently, Ayato et al. (2006) studied Pt electrode/Nafion interface in $HClO_4$ aqueous solutions using surface-enhanced infrared absorption spectroscopy (SEIRAS) with the aim of investigating the structure of the interface. They inferred the $-SO_3^-$ groups in Nafion act like counterions at the Pt/ionomer interface to form the electric double layer, due to flexibility of the pendant side chains of the ionomer membrane.

2.2.4.2 Driving Forces for Proton Transport

When a fuel cell is working at steady state, electronic current in the external circuit must equal to ionic current in the electrolyte. As is well known, it is potential difference between anode and cathode that drives electrons through the external load. Then, what is the driving force for ionic transport in a fuel cell?

The flux of protons through the membrane in a PEM fuel cell can be described using the Nernst-Planck equation (Strathmann, 2004):

$$J_i = -D_i \frac{dC_i}{dx} - D_i \frac{z_i C_i F}{RT} \frac{d\Phi}{dx} + v_k C_i \qquad (2.9)$$

where J_i is flux of species i (mol/cm^{2}s); D_i is diffusivity of species i (cm^2/s); C_i is the concentration of i (mol/cm^3); v_k is the velocity (m/s); Φ is electrical potential (V); z_i is charge on species I; and x is distance in the direction of diffusion of species i (cm).

This equation considers three modes of ion transport in polymer electrolyte. The first term $D_i \frac{dC_i}{dx}$ represents the diffusion, the second term $D_i \frac{z_i C_i F}{RT} \frac{d\Phi}{dx}$ the migration, the third term $v_k C_i$ the convection. That is to say, there are three driving forces for proton transport: an internally generated electrical potential gradient, due to electrochemical reactions in the anode and cathode, will exist to create migration, a proton concentration gradient will exist to create diffusion of protons from the anode to the cathode, and diffusion and absorption of water in the membrane will lead to a convective proton flux. There is a very limited understanding of the interaction of migration, diffusion and convection processes (Amphlett et al, 1995).

2.2.4.3 Proton Transport in Biofuel Cells

The limited reports on proton transport in biofuel cells are only focused on microbial fuel cells so far. Gil et al. (2003) observed a decreasing pH in the anode chamber and an increasing pH in the cathode chamber during operation of a two-chamber microbial fuel cell, because proton transport through the Nafion seemed to be slower than the proton production rate in the anode chamber and the proton consumption rate in the cathode chamber.

The same results were found in our experiments. Moreover, the sodium ions in the membrane were found to hinder proton transport. The cathode overpotential increased in the presence of sodium ions in the membrane and at the cathode. In the process of our study, we found similar work has been reported for microbial fuel cell systems in

September, 2006 (Rozendal et al., 2006). Our results confirm the conclusions of Rozendal et al. (2006)

Rozendal et al. (2006) observed that during operation of a microbial fuel cell mainly cation species other than protons were responsible for the transport of positive charge through the membrane, which resulted in accumulation of these cations and in increased conductivity in the cathode chamber. Furthermore, protons are consumed in the cathode reaction and, consequently, transport of cation species other than protons resulted in an increased pH in the cathode chamber and decreased cell performance. Cation transport in membrane, therefore, needs to be considered in the development of future microbial fuel cell systems.

For the construction of a complete biofuel cell, it is mandatory to couple the anode and cathode units. The anolyte and catholyte solutions are normally compartmentalized. Proton exchange membrane, such as Nafion, is extensively used in biofuel cells to provide a separation between fuel and oxidizer, but at the same time facilitates transport of positive charge to compensate for transport of electrons. However, if the bioelectrocatalytic reactions are made indifferent to the interfering components, non-compartmentalized fuel cells will become feasible.

A non-compartmentalized enzymatic biofuel cell employing glucose and O_2 as fuel and oxidizer, and using PQQ-FAD/GOx and Cyt c/COx functionalized Au-electrodes as biocatalytic anode and cathode, was reported by Katz et al.(2003). Since the reconstituted GOx provides extremely efficient biocatalyzed oxidation of glucose that is unaffected by oxygen, the anode can operate in the presence of oxygen.

A single-chamber microbial fuel cell in the presence and absence of a Nafion membrane was operated by Liu and Logan (2004). They observed a reduced power output when the membrane was present. Potential measurements showed that the anode potential

as identical in the presence and absence of the membrane, but that the cathode potential was lower when the membrane was present.

In literature, the Nafion membrane was used in H^+-form (Liu and Logan, 2004; Liu et al., 2004) or Na^+-form (Rabaey et al., 2003, 2005) for compartmentalized microbial fuel cells.

2.2.5 Mass Transport

When an enzymatic fuel cell is operating, a liquid environment is needed to maintain enzyme activity. Organic fuel, such as sugar or alcohol, has enough high solubility. Thus, sufficient fuel supply is easily maintained in biofuel cells. The problem is at the cathode side. Oxygen is generally used as a reductant in biofuel cells. Glucose solubility is 910 g/L, whereas oxygen solubility is only 8.24 mg/L at 25°C in water (Figure 2.8). Transport of oxygen within a biocatalyzed cathode is considered to be a significant rate-limiting step (Barton, 2005), especially when the oxygen is present in aqueous solution. Oxygen transport limitation will lead to a significant concentration voltage loss.

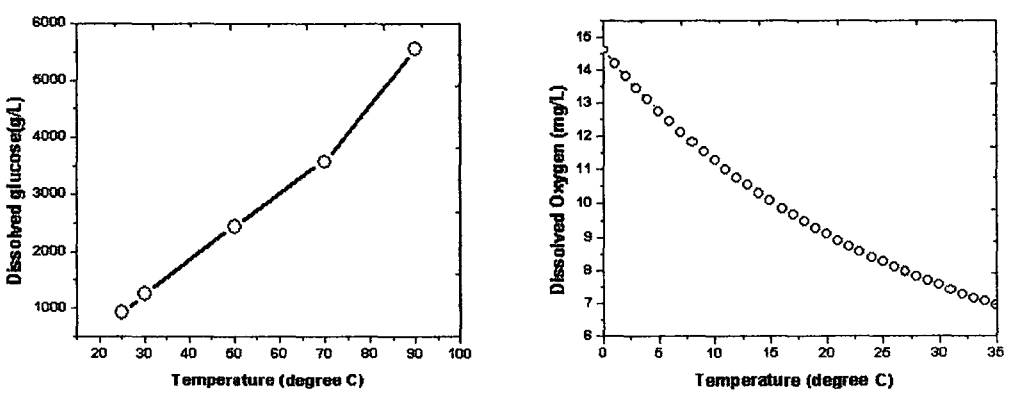

(a) (b)

Figure 2.8 (a) Glucose solubility in water (b) Oxygen solubility in water

Based on this, Barton (2005) proposed a one-dimensional model, which predicts a maximum current density of near 100 mA/cm^2 for a 300 μm thick O_2-breathing composite bio-cathode (Figure 2.9).

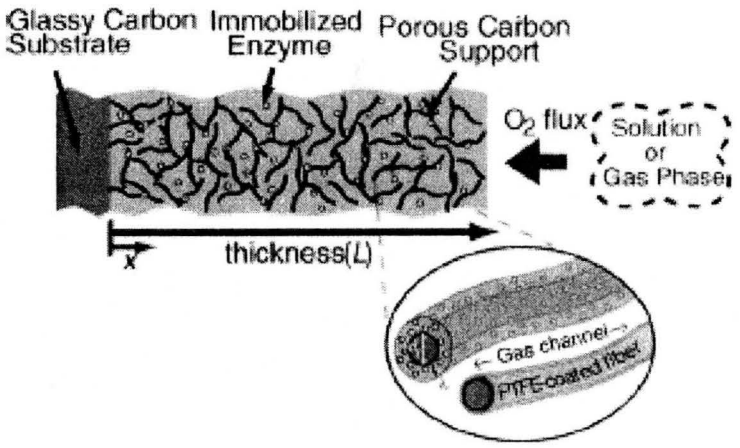

Figure 2.9 One-dimensional model for a composite mediated bio-cathode (Barton, 2005)

2.2.6 Internal Resistance

Fuel cells are inherently low-voltage devices. So, the significant losses will be present in a fuel cell if its internal resistance is high. People still confuse internal resistance with the total resistance in biofuel cells. Some researchers believe internal resistance means ohmic resistance (Rabaey et al., 2005; Aelterman, et al., 2006); whereas others think of the internal resistance as the total resistance, including activation, ohmic and concentration resistances (He et al., 2005; Alferov et al., 2006).

According to Fuel Cell Glossary, internal resistance is defined as losses caused by internal structures that create resistance to the flow of ions in the electrolyte and resistance to flow of electrons through the electrode. Based on this, internal resistance refers to ohmic resistance in this thesis.

The typical value of internal resistance is 0.245 Ωcm^2 for PEMFCs, 2 Ωcm^2 for

SOFCs (Larminie and Dicks, 2003). The internal resistance of biofuel cells is much higher. According to Figure 2.2 (Tsujimura et al., 2002), the internal resistance of the glucose/O_2 biofeul cell was 450 Ωcm^2.

Persson et al. (1985) and He et al. (2006) proposed the internal resistance was the main current-limiting factor in biofuel cells.

2.3 Rate-limiting Step and Overpotential

A simple equivalent circuit model of a fuel cell is shown in Figure 2.11 (Larminie and Dicks, 2003). The resistor R_{ohm} models the ohmic losses. The resistor R_{act} and R_{conc} model the activation losses and the concentration losses, respectively. The capacitor models the double layer on or near the electrode-electrolyte interface. According to Figure 2.10, R_{ohm}, R_{act} and R_{conc} are found to be connected in series.

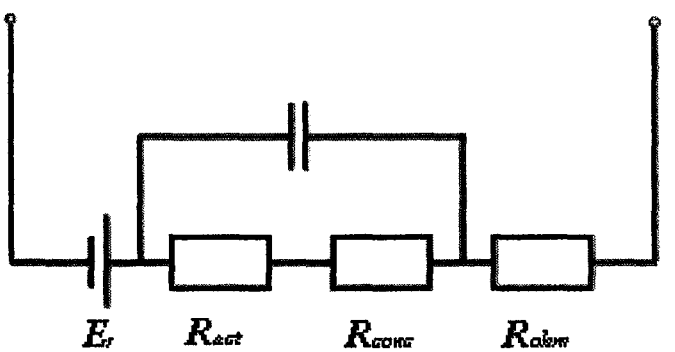

Figure 2.10 A simple equivalent circuit model of a fuel cell (Larminie and Dicks, 2003)

When a load is connected in external circuit, a constant current will flow in the whole circuit at steady state. The product of current and R_{act}, R_{ohm} and R_{conc} are η_{act}, η_{ohm}, η_{conc} in fact, respectively. Thus, we have

$$I = \frac{\eta_{act}}{R_{act}} = \frac{\eta_{ohm}}{R_{ohm}} = \frac{\eta_{conc}}{R_{conc}} \tag{2.11}$$

If one of the resistors is significant, the overall resistance of the internal circuit is approximately given by the biggest resistance. That is to say, the biggest resistor bears the rate-limiting step. According to Eq.2.11, the overpotential related to the largest resistor will be significant. Therefore, the largest overpotential is associated with the rate-limiting step in a fuel cell. Overpotential corresponds with resistance.

Current interruption method and electrochemical impedance spectroscopy (EIS) are two widely used methods to distinguish between different overpotentials for the whole cell (Larminie and Dicks, 2003), whereas reference electrode method allows tracking the performance of the cathode and anode independently to determine the overpotentials at each electrode (Choban, et al., 2005).

2.4 Current Interruption (CI) Method

The current interrupt method measures the responses of potential relaxation from steady-state polarization to open-circuit conditions (Lee et al., 1998). Therefore, it includes the relaxation processes of various overpotentials, which are composed of activation overpotential (η_{act}), ohmic overpotential (η_{ohm}) and concentration overpotential (η_{conc}). Suppose a fuel cell is providing a current at which the concentration overpotential is negligible. Only ohmic losses and activation losses will cause the voltage drop. When the current is suddenly cut off, according to Figure 2.10, the charge double layer will take some time to disperse, and thereby the associated overpotential. However, the ohmic losses will immediately reduce to zero. A voltage change against time is expected as in Figure 2.11 after a current interruption. Ohmic and activation overpotentials are thus distinguished clearly.

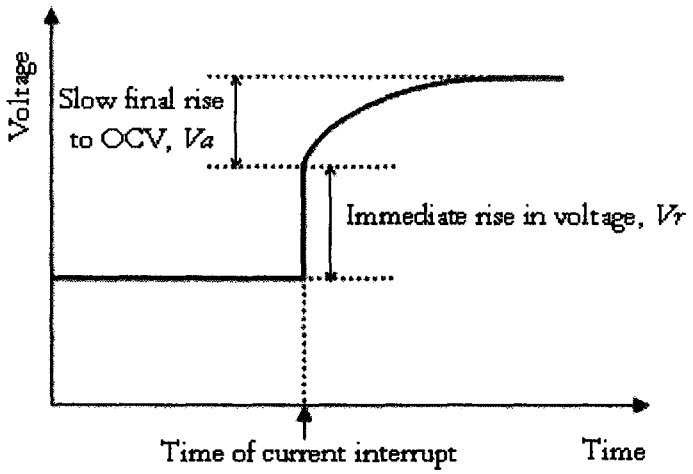

Figure 2.11 Sketch graph of voltage against time for a fuel cell after a current interrupt (Larminie and Dicks, 2003)

Lee et al. (1998) employed a current interrupt method to characterize a molten carbonate fuel cell. The ohmic overpotential, activation overpotential and even Nernst loss were successfully separated in detail. To the best of our knowledge, this method has not yet been used in biofuel cells so far.

2.5 Electrochemical Impedance Spectroscopy (EIS) Method

The principle of this method is the application of a small sinusoidal perturbation potential at different frequencies to the fuel cell. The response is an alternating current (ac) signal of the same frequency with a possible shift in phase and change in amplitude. The ac response of the fuel cell provides additional information on the investigated system. By the analysis of the impedance spectra, it is possible to separate the individual voltage losses of the single components, such as the anode, cathode and electrolyte, and perhaps even to identify diffusion process. The rate-limiting step can be determined from these results in a fuel cell (Barsoukov and Macdonald, 2005).

The correlation between impedance measurements and IV curve was first described by Wagner (2002) and given schematically in Figure 2.12. The polarization resistance or total resistance of the cell (R_{Cell}) measured at *Un* corresponds to the tangent to the IV curve at that potential. The polarization resistance of the cell is the impedance at frequencies near 0 Hz where only ohmic parts attract attention, which can be obtained by extrapolating simulated impedance at very low frequency or summing the individual resistances, obtained after fitting the measured spectra with an equivalent circuit. Using these impedance parameters we can calculate the overpotentials at the components of a fuel cell. These voltage losses and the cell voltage can be calculated from the product of the ohmic components magnitude and the current densities (Wagner et al., 1998), as shown in Figure 2.13.

EIS provides an effective method to probe the electron transfer resistances at electrodes, especially when the slow electron transfer between biocatalysts and electrodes was always thought one of critical challenges in developing biofuel cells (Persson et al., 1985; Kim et al., 2006). The impedance measurements can be done between the anode and cathode of fuel cell (two-electrode mode) or for each electrode using a counter electrode and a reference electrode (three-electrode mode) in biofuel cells (Katz and Willner, 2003). The overall electron-transfer resistance of the fuel cell derived from the EIS by using two-electrode mode is composed of both of electron transfer resistances of the anode and the cathode, which are separated by using three-electrode mode.

In biofuel cells, Wang et al.(2005) used three-electrode mode to investigate the electron transfer resistance of the individual carbon nanotube modified electrode; He et al. (2006) separated the electrolyte resistance, electron transfer resistance and diffusion resistance of a microbial fuel cell using two-electrode mode (Figure 2.14).

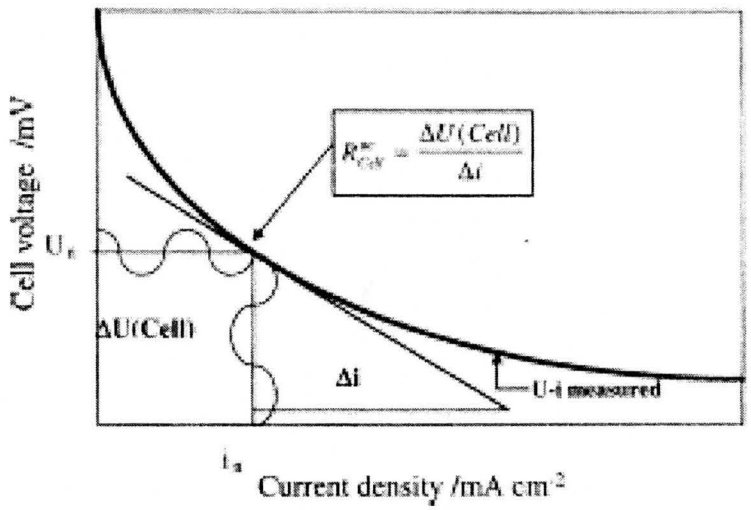

Figure 2.12 Schematic of the correlation between impedance of a fuel cell and IV curve (Wagner, 2002)

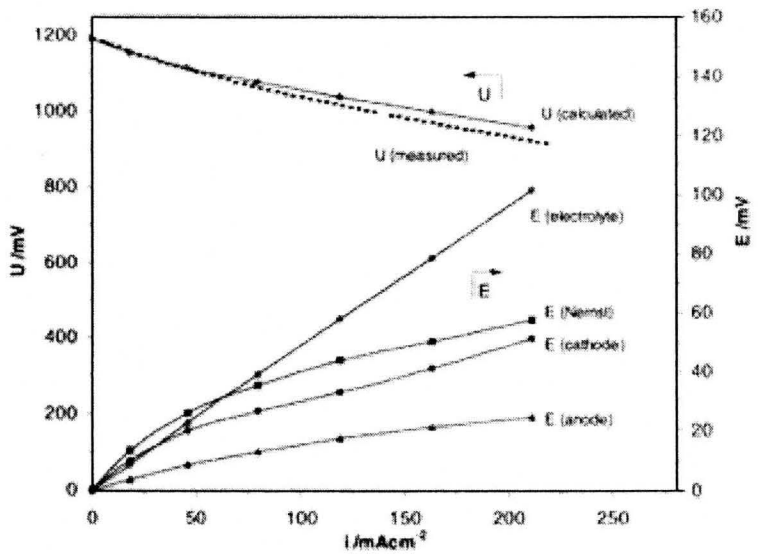

Figure 2.13 Overpotentials at a SOFC as a function of current density (Wagner et al., 1998)

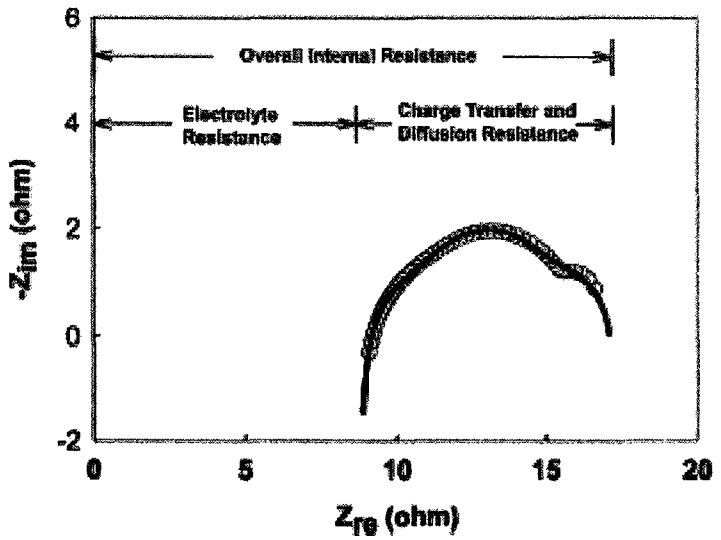

Figure 2.14 Nyquist plots of impedance spectra of an up-flow microbial fuel cell (He et al., 2006)

2.6 Reference Electrode Method

In most conventional fuel cells, the only potential that can be measured is the difference between the anode and the cathode and its change upon the application of a load. This overall cell potential does not provide thorough insight into the reasons of limiting factors at the individual electrode. One would prefer to track the performance of the cathode and anode independently to determine the overpotentials at each electrode, and whether the fuel cell is either kinetically or mass transfer limited at the anode or cathode or both. Reference electrode method allows for independent, direct evaluation of each electrode performance (Choban, et al., 2005).

In the literature, there were several reference electrode configurations in conventional fuel cells. Thomas et al. (2002) used a gaseous dynamic hydrogen electrode (DHE) as a reference in PEM-based fuel cells. Han et al. (2003) developed a new evaluation of anode/cathode performance by using MEA combined with a gold wire used

as reference electrode. He and Nguyen (2004) integrated a reference electrode by using a strip of Nafion as the electrolyte to connect the reference electrode directly with MEA thereby eliminating the need to modify the typical PEM fuel cell setup. Choban et al. (2005) introduced an external Ag/AgCl reference electrode to determine the limiting factors of laminar flow-based membraneless microfuel cells.

In view of the all-liquid nature of biofuel cells, it is easy to introduce an external reference electrode. Willner et al. (1998) and Liu and Logan (2004) used a saturated calomel electrode (SCE) and Ag/AgCl reference electrodes to separate anode and cathode overpotentials in biofuel cells, respectively.

Two kinds of IR drops need to be paid more attention to when we use the reference electrode to separate anode and cathode overpotenatials. If a current is passed between anode and cathode, a voltage drop across both electrodes arises. The ideal location for potential measurement now should be inside the double layer at the electrode. At any other place, part of the voltage drop between anode and cathode is added to reference potential. Therefore, reference electrode should be as close as possible, such as 0.5 to 1mm, to the working electrode to reduce the error. Another thing is whether or not the relative potentials measured between working electrode and reference electrode represent potentials of the individual electrodes alone depends in part on the composition/conductivity of the electrolyte that separate the anode and the cathode, especially when only one reference electrode is employed, such as the case described by Choban (2005). Only when the electrolyte has high conductivity and the potential drop across the electrolyte between anode and cathode is negligible, can potential differences measured between working electrode and reference electrode be attributed exclusively to the working electrode.

Chapter 3 Experimental Details

3.1 Biofuel Cell Design and Construction

A schematic of biofuel cell design is shown in Figure 3.1. Our biofuel cell is composed of a bio-anode and a conventional, platinum-based cathode. The anode and cathode compartments are separated by a half Membrane-Electrode-Assembly (MEA). The anode and cathode compartments (working volume of 45ml each) were made from plexiglass tube. Each side of plexiglass tube was fitted with two ports. These ports serve as gas and electrolyte inlets and outlets. The two graphite plates (Speer Canada Inc., Canada) with 21× Φ2 mm holes serve as anode in the anode compartment and a current collector and backing plate in cathode compartment, respectively. Platinum wire connecting graphite plates passes through ports at plexiglass tube to be connected in the external circuit. Two carbon papers, one used as a gas diffusion backing and to provide a good electrical contact at the cathode, and another used to protect the membrane at the anode, are placed into the fuel cell housing during the installation of cell. There are two O-rings on plexiglass covers and four O-rings on Teflon plates to provide an electrolyte tight seal. The two 3.9375"×3.937"×0.5"Teflon plate and two stainless steel covers are to tighten plexiglass tube and two Teflon plates by six fastening parts consisting of bolts, washers and nuts. Thus, a good electrolyte tight seal and a good electrical contact are attained. The effective operating area of this cell is 0.66 cm^2.

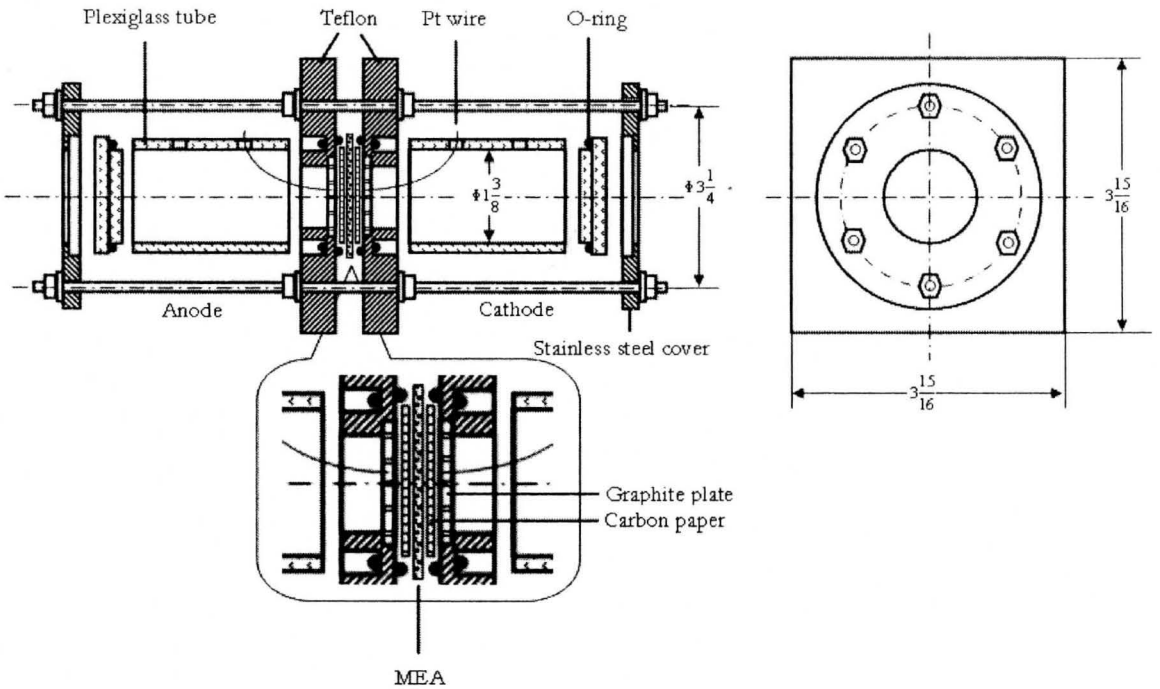

Figure 3.1 Schematic diagram of our biofuel cell

3.2 Membrane-Electrode-Assembly (MEA) Preparation

3.2.1 Membrane Pretreatment Procedure

The PEM (Nafion 117) was purchased from DuPont. The membrane was pretreated with a standard clean procedure by: (i)boiling in 3% hydrogen peroxide for 1 h to oxidize organic impurities; (ii)rinsing with boiling water for several hours; (iii)boiling in 1M sulfuric acid for 1h to remove any metallic/ionic impurities; and (iv)rinsing again in boiling water to remove any excess acid.

3.2.2 Electrode Ink Preparation

A Nafion/Pt-C/glycerol ink was prepared from a Nafion solution (5 wt%) and 19.8 wt% Pt on carbon combined with glycerol and water, and then thoroughly mixed by ultrasound. The 5 wt% Nafion solution was purchased from Solution Technology Inc.,

and the 19.8 wt% Pt on carbon was purchased form Etek Inc. The preparation procedure was as follows:

1. Mixed 5 wt% Nafion solution and 19.8 wt% Pt on carbon with a weight ratio of 1:3 for the Nafion (dry)/Pt-C.

2. Added water and glycerol such that the weight ratios are approximately 1:5:20 for carbon/water/glycerol.

3. Mixed extensively with ultrasound.

3.2.3 Membrane-Electrode-Assembly (MEA) Preparation

After preparing the electrode ink, a half MEA was made by paint and peel hot pressing technique:

1. A blank Teflon film was thoroughly cleaned and coated with a thin layer of mold release spray. The blank was painted with a layer of ink, and baked in an oven at 120℃ until dry. If necessary, additional layers were added to achieve the catalyst loading of 0.4 mg/cm^2 Pt.

2. The coated blank and a membrane were placed in a hot press at 120℃, and pressed at 70～90 atmosphere for 90 seconds.

3. The assembly was removed from the press and allowed to cool, and then the Teflon blank was peeled from the membrane leaving the thin film adhering to the membrane.

After that, post-treatment of MEA could be done by the following two methods prior to get H^+-form MEA and Na^+-form MEA:

1. Lightly boiling the MEA in 0.5 M H_2SO_4 for 1h and rinsing in de-ionized water for 1 h.

2. Lightly boiling the MEA in a 0.1 M phosphate buffer at pH7 for 1h and rinsing in de-ionized water for 1 h.

3.3 Buffer, Fuel, Mediator, Enzyme and Electrode Preparation

Glucose oxidase (GOx) (E.C. 1.1.3.4) was from Biocatalysts Limited, UK with activity of 1,650 U/g (1U corresponds to the amount of the enzyme which oxidizes 1 μ mol glucose per min at pH = 7.0 and 25℃);

Phosphate buffer solution (0.1 M, measured pH 7.40) was made from Na_2HPO_4 and NaH_2PO_4, which were purchased from Sigma-Aldrich, Canada.

Tris buffer solution (0.1 M, measured pH 7.42) was made from Tris and HCl, which were purchased from Sigma-Aldrich, Canada.

β -d-glucose was obtained from Sigma-Aldrich, Canada. The β -d-glucose solution in the phosphate buffer was allowed to mutarotate for 24 h before use.

Ferrocene monocarboxylic acid (FMCA) was chosen as mediator and obtained from Sigma-Aldrich, Canada. The FMCA was dissolved in the phosphate buffer for use.

The graphite plate in anode compartment was cleaned with 1.0 M NaOH followed by 1.0 M HCl after each experiment and stored in distilled water before use.

All solutions were prepared with DI water.

3.4 Experimental Set-up

Figure 3.2 shows the experimental set-up for the biofuel cell operation and measurement apparatus. The anode compartment was kept anoxic by purging nitrogen gas. Oxygen or air was purged into the cathode compartment. The gassing rate to each compartment was 10 ml/min. The biofuel cell was placed in a temperature-controlled water bath. The variable resistance for the testing cell was controlled by a variable resistor. Multimeters were used to measure the cell current, voltage and potential difference between electrodes and the reference electrode. A LCR meter was used to measure the cell impedance. A pH meter was used to monitor the pH value change in the anode compartment, and a reference electrode was used to determine the overpotentials at

each electrode. Experimental data acquisition in a personal computer was controlled by general purpose interface bus (GPIB) interface, along with programs written in Quick Basic as experiment progressed.

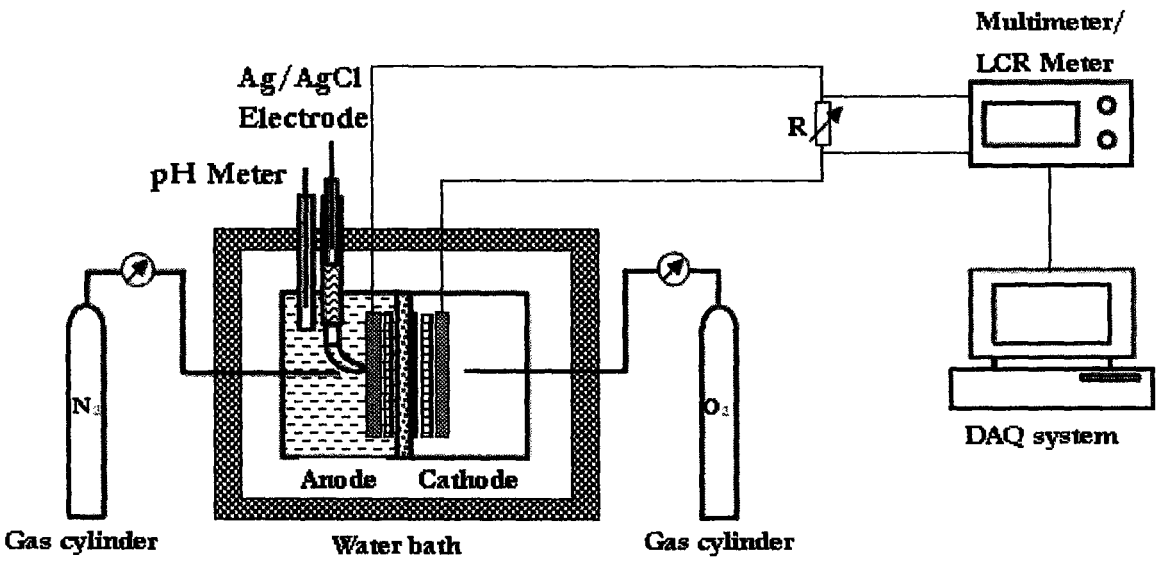

Figure 3.2 Schematic of biofuel cell operation and measurement apparatus

3.5 IV Curve Measurement

Cell current and voltage were measured with HP 3478A multimeter (Electrolab Inc., USA) from open-circuit to short-circuit. The biofuel cell was allowed to equilibrate at open circuit for around 0.5~1 h, until the open circuit potential stabilized. The resistance between electrodes was lowered stepwise, pausing at each resistance setting for 5 min. The cell current and voltage were measured and recorded at the same time intervals, assuming a steady state was reached. Generally, it took around 1 h to take one IV curve measurement. The power extracted from the biofuel cell was obtained by $V_{cell} \times I_{cell}$. The current and power densities were then obtained by the cell current and power divided by the cell effective operating area.

3.6 Electrochemical Impedance Spectroscope (EIS) Measurement

To carry out the EIS measurements, a HP 4284A LCR meter (Test Equipment Connection, USA) was employed, which was connected directly with the biofuel cell. The R-X mode of measuring the real and imaginary parts of the complex impedance of biofuel cell was chosen. Thirty-eight frequencies ranging from 20 Hz to 100 KHz were used at each measurement. The amplitude of the sinusoidal potential was 10 mV. The bias voltage was 0 V.

The biofuel cell is an active cell, which will deliver power to HP 4284A LCR meter. According to HP 4284A LCR meter manual, a DC current source or a charged capacitor is not allowed to directly connect to the machine. However, the maximum current of our biofuel cell is only around 1.5 mA. The tiny current should have no damage to the machine, which was confirmed by Agilent Technologies.

EIS measurements involved excitation of the device under test (DUT) by an a.c. voltage of small amplitude and evaluation of the corresponding response. If a safe d.c. current is added in the circuit at steady state, there are no effects on the impedance measurement results of DUT, especially for a fuel cell in theory. Actually, PGSTAT30, a very popular instrument, which is capable of measuring impedances, can be used to measure the impedance of some electrochemical cells, such as batteries and fuel cells, which are capable of delivering power to PGSTAT30 from Autolab/PGSTAT30 manual. This is allowed only to a maximum power of 13 W.

To guarantee correct measurement results, the impedance of a Dummy cell and the Dummy cell connected with a 1.5 V battery in series was measured. The results were shown in Figure 3.3. There was not a big difference between the two devices. HP 4284A LCR meter could be used to measure the impedance of our biofuel cell.

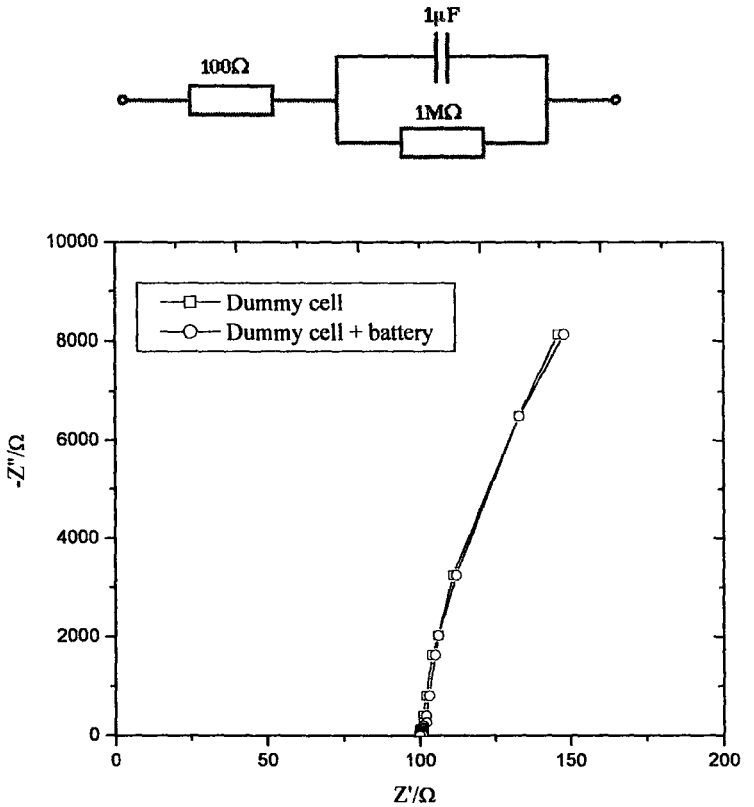

Figure 3.3 Impedance measurement results for a Dummy cell and the Dummy cell connected with a battery in series

What we have to mention is, when the LCR meter with an output resistance of 100 Ω was directly connected to the biofuel cell to do the impedance measurement, the impedance was measured at some point in the IV curve of the biofuel cell with a load of 100 Ω, not at open circuit.

3.7 Overpotential Measurement

Two kinds of reference electrodes, Ag/AgCl/KCl (saturated) reference electrode method (Figure 3.4) and Au reference electrode method (3.6), were employed in overpotential measurements. In Figure 3.4, it was easy to introduce a commercially

available external reference electrode, such as an Ag/AgCl electrode, into the anode chamber to separate the anode and cathode overpotentials. The anode potential (V) vs. this reference electrode was measured when doing current-cell voltage (V_{cell}) measurements. The cathode potential could then be obtained by adding the anode potential to the cell potential. Finally, the anode and cathode polarization curves were obtained, respectively. To verify the validity of the method in Figure 3.4, another Ag/AgCl reference electrode was introduced to the cathode chamber to measure the potential of cathode vs. reference electrode after 0.1 M NaCl solution had been added in the cathode chamber. The results for one Ag/AgCl electrode in comparison with two Ag/AgCl electrodes were shown in Figure 3.5. When current density was less than 0.16 mA/cm^2, the results agreed with each other. When current density increased, the deviation increased, due to the increasing IR drop in the electrolyte. However, the maximum deviation was only around 20 mV; Moreover, the cathode potential had the same trend with increasing current density whether with one Ag/AgCl electrode or two. Therefore, one Ag/AgCl reference electrode would provide a reliable means of recording potential differences between the reference electrode and the anode or cathode, respectively, in our biofuel cell, especially when a gas cathode was used at the cathode.

The electrolyte at the anode chamber has to have a strong ionic strength (a measure of how ionic a solution is) for the application of an Ag/AgCl electrode; otherwise, there will be a big junction potential between the reference electrode and the electrolyte, which will affect the reliability of experimental results. In some cases, DI water was used as electrolyte in our biofuel cell. An Ag/AgCl electrode could not be employed to separate the anode and cathode performance. Therefore, we have to resort to another reference electrode method. The fabrication procedure of an Au reference electrode and measurement of potential difference between the anode, cathode and pseudo reference electrode in the biofuel cell are shown in Figure 3.6. V_{Cell}, V_{Anode}

$V_{Cathode}$ indicated the potential difference between anode and cathode, that between anode and Au reference electrode and that between cathode and Au reference electrode, respectively.

The detailed fabrication procedure of the Au reference electrode was as follows:

1. After two pieces of Nafion were cleaned according to procedure 3.2.1, one of them was laid on a polymer film. A Φ0.3 mm gold wire was centered upon the wet membrane;

2. Next, a 5 wt% Nafion solution was lightly heated to be thicker, and then spread out on the wet membrane, which was then covered with another wet membrane;

3. The two membrane sheets with gold wire were pressed together and then put in a vacuum furnace of 0.01 Pa at 80°C for 6 h;

4. A sandwich thick electrode membrane was made with a gold wire. Following the MEA preparation procedure described in 3.2.3, a thicker half MEA with an Au reference electrode was ready for use.

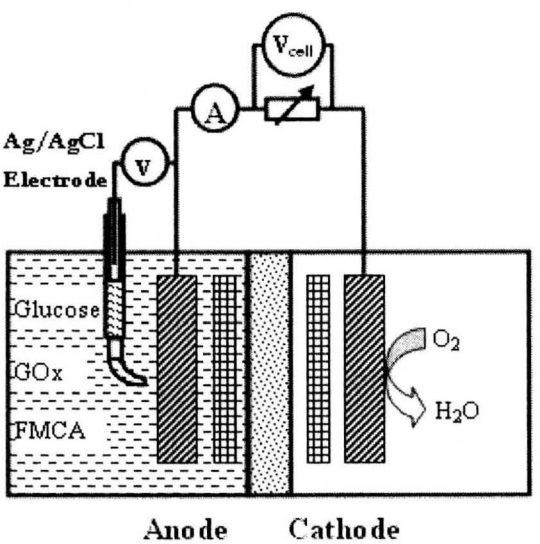

Figure 3.4 Schematic of the biofuel cell with an external Ag/AgCl reference electrode and measurement of V_{Anode} and V_{Cell} in the biofuel cell

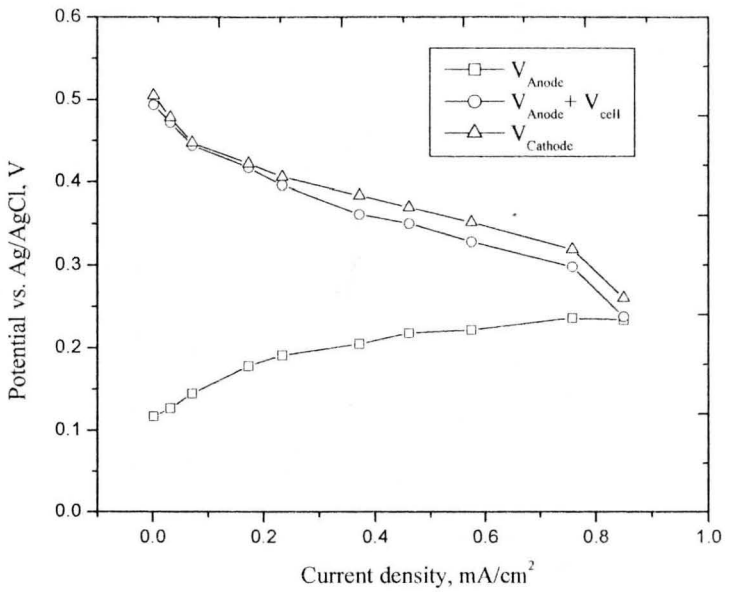

Figure 3.5 Electrode overpotentials measured by one or two Ag/AgCl reference electrodes

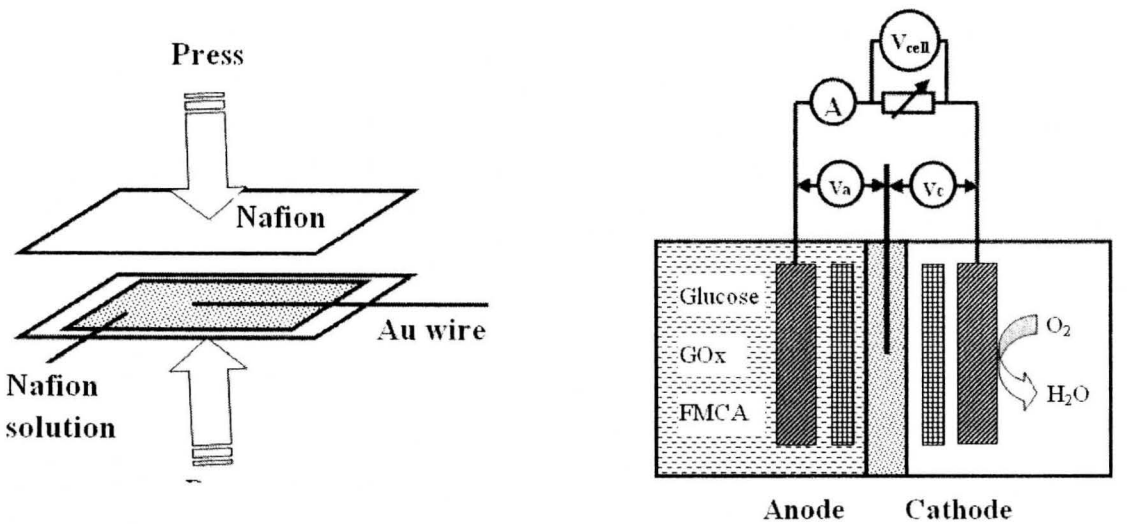

Figure 3.6 Schematic of the fabrication procedure of MEA with Au reference electrode (Han et al., 2003) and measurement of V_{Cell}, V_{Anode} $V_{Cathode}$ in the biofuel cell

3.8 pH Value Measurement

The pH values of electrolyte and buffer were measured with VWR - SB20 Symphony pH meter (VWR International, Canada).

Chapter 4 Results and Discussion

4.1 Rate-limiting Step Survey

To get some perceptual knowledge of possible limiting steps in the biofuel cell, the cell was examined under following different operating conditions: 1) glucose concentration; 2) GOx concentration; 3) FMCA concentration; 4) anolyte; 5) membrane form; 6) oxygen supply rate. Due to the poor reproducibility of experiments, glucose was added in the anode chamber in sequence, after each IV curve measurement. GOx and FMCA were also added in this way to check the effects of GOx and FMCA concentration on the cell performance, respectively. Unless otherwise noted, the biofuel cell was working with 1 g GOx, 4 mM FMCA and 200 mM glucose in 0.1 M phosphate buffer in anode chamber, and 10 ml/min oxygen supply rate at 25°C. The anode compartment was purged by nitrogen at the same flow rate. The membrane was treated by 0.5 M H_2SO_4.

Figure 4.1 shows the effects of glucose concentration on the cell IV curve and power density. When glucose concentration increased, the performance of the biofuel cell unbelievably decreased. The open circuit potential (OCP), maximum current density and power density of the biofuel cell decreased from 0.421 V, 2.315 mA/cm^2 and 0.176 mW/cm^2 to 0.361 V, 0.971 mA/cm^2 and 0.059 mW/cm^2, respectively, when glucose concentration increased from 25 mM to 200 mM. The Nernst equation for the anode reaction in Eq. 1.1 is shown as follows:

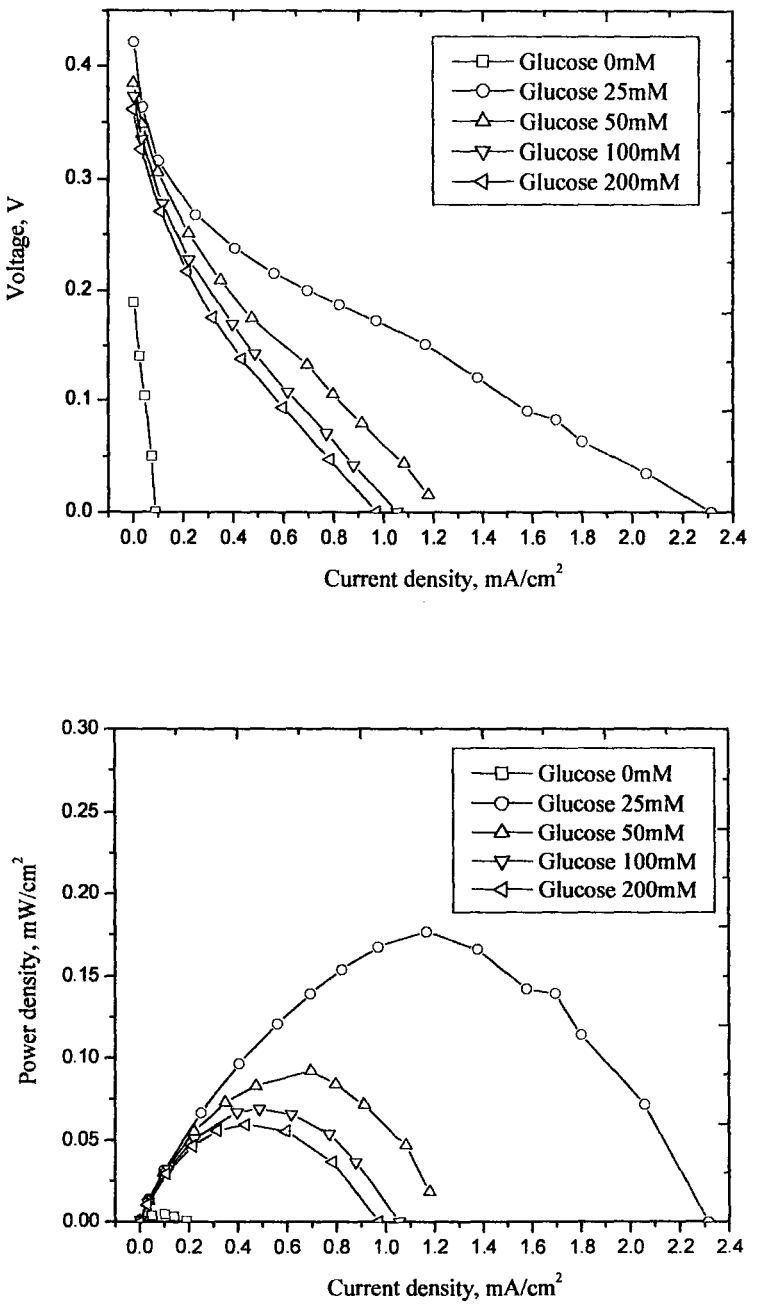

Figure 4.1 Current–voltage behavior and power density of the biofuel cell at different external loads with different glucose concentration

$$E_a = E^0 - \frac{RT}{4F} \ln \frac{[a_{H^+}]^4 [a_{\delta-gluconolactone}]^2}{[a_{glucose}]^2} \quad (4.1)$$

where a represents the chemical activities of all of the species which appear in the anode reaction.

According to Eq. 4.1, the anode potential E_a should increase with the increasing glucose concentration, assuming a constant pH value and δ-gluconolactone concentration. Gil et al. (2003) and Liu and Logan (2003) studied the effect of fuel concentration on the maximum current and the OCP in microbial fuel cells, respectively. They found the current and voltage followed saturation kinetics as a function of fuel concentration.

When the concentration of GOx increased, the performance of the biofuel cell first increased, and then decreased (Figure 4.2). The maximum OCP of 0.354V, current density of 1.159 mA/cm^2 and power density of 0.070 mW/cm^2 were obtained with 0.6 g GOx used as catalyst. The poor performance of the biofuel cell with high GOx concentration might be due to the nonconductive protein shell sticking on the anode.

The OCP, maximum current density and power density of the biofuel cell continuously increased from 0.485 V, 0.878 mA/cm^2 and 0.076 mW/cm^2 to 0.528 V, 1.308 mA/cm^2 and 0.113 mW/cm^2, respectively, when FMCA concentration increased from 0.27 mM to 4 mM, as shown in Figure 4.3, which confirms that the electron transfer is the rate-limiting step in biofuel cells. However, the solubility of FMCA in phosphate buffer is limited. The maximum solubility of FMCA in phosphate buffer is around 4 mM.

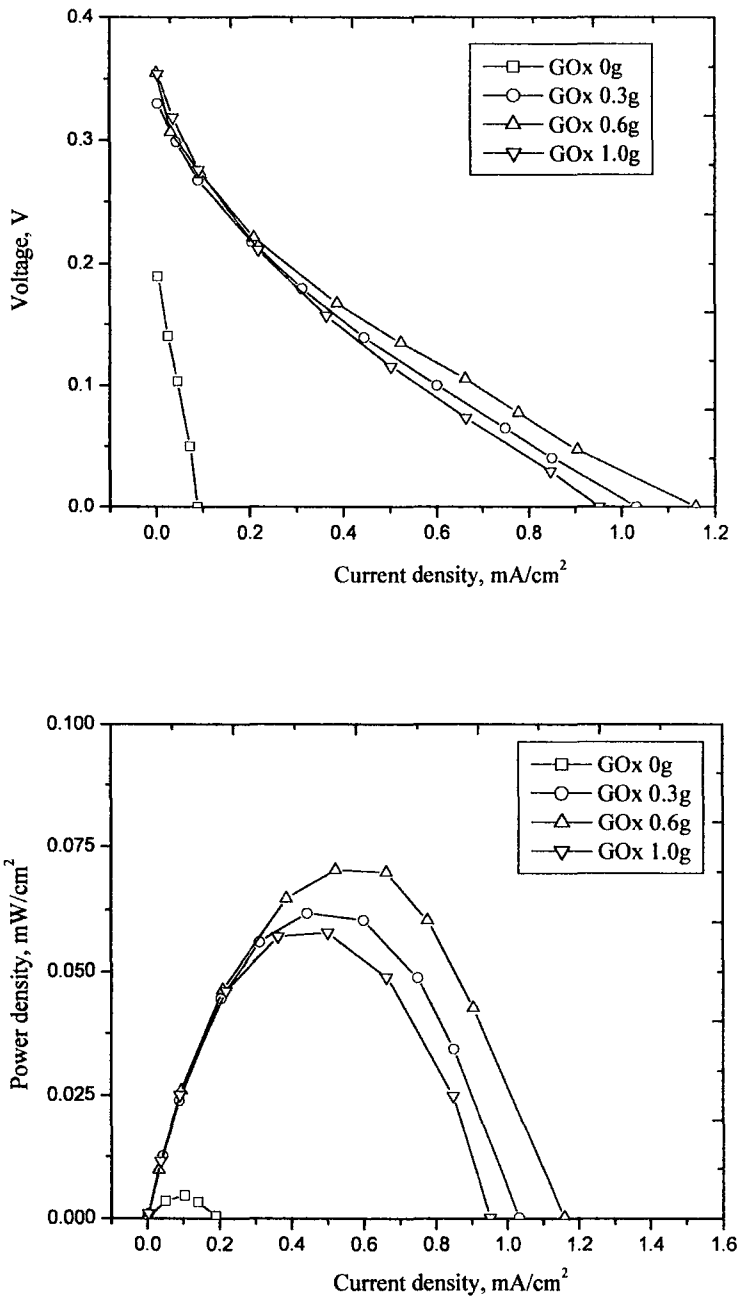

Figure 4.2 Current–voltage behavior and power density of the biofuel cell at different external loads with different GOx concentration

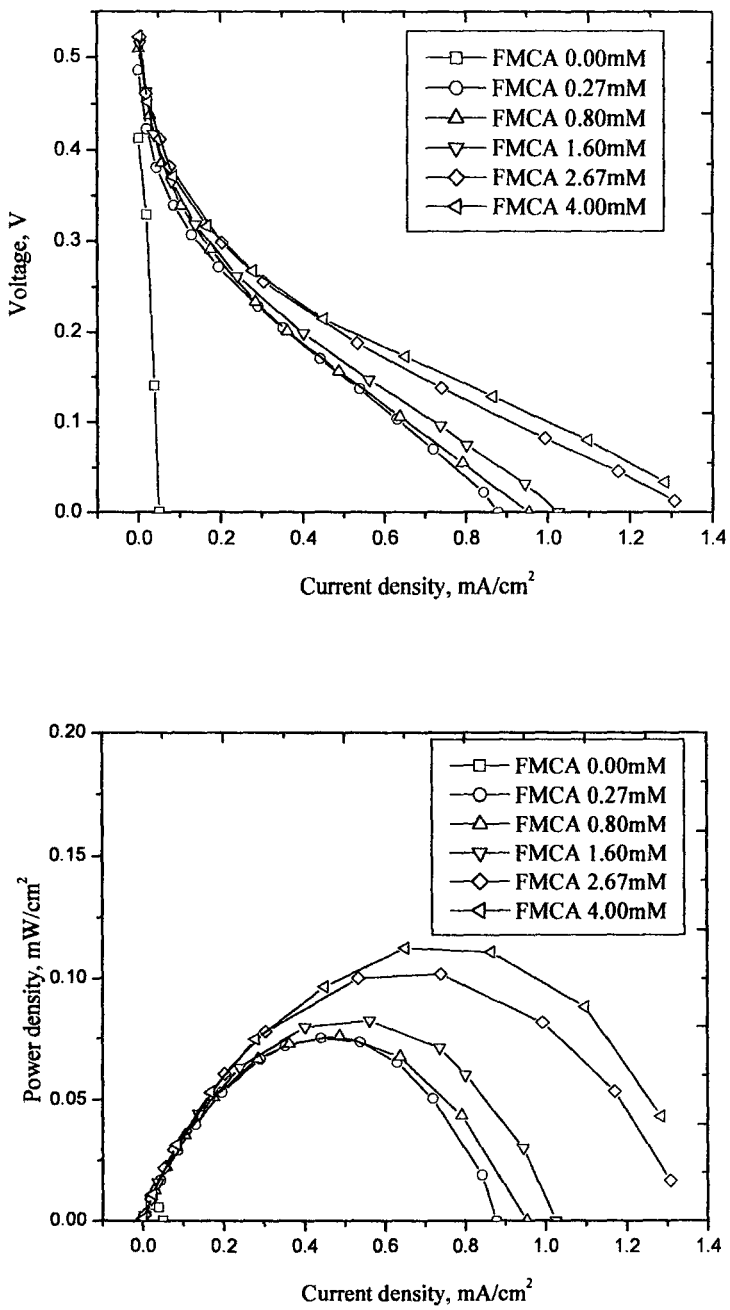

Figure 4.3 Current–voltage behavior and power density of the biofuel cell at different external loads with different FMCA concentration

The cell had very poor performance operated using DI water in comparison with phosphate buffer in the anode chamber (Figure 4.4). The OCP, short circuit current density and maximum power density of the cell were 0.285 V, 0.235 mA/cm^2, and 0.015 mW/cm^2, whereas they were 0.438 V, 1.780 mA/cm^2, and 0.126 mW/cm^2 using 0.1 M phosphate buffer as anolyte. The results agree with that of Gil et al. (2003). The purpose of application of buffer in biofuel cells is to provide a living environment for biocatalysts (pH=7). Another important thing is the mediator, FMCA, has a good solubility in phosphate buffer (around 4 mM). In contrast, FMCA hardly dissolves in DI water. This will hinder electron transfer rate at anode, thus affecting the cell performance.

The biofuel cell with Na^+-form membrane also had poor performance, including the OCP of 0.285 V, maximum current density of 0.139 mA/cm^2 and power density of 0.006 mW/cm^2, in comparison with H^+-form membrane (Figure 4.5). In the literature, Rabaey et al. (2003, 2005) used Na^+-form membrane in their microbial fuel cells. But they did not give the reason why they used Na^+-form membrane.

The biofuel cell performance operated with air-breathing or 10 ml/min oxygen at the cathode was shown in Figure 4.6. The OCP of the cell with oxygen cathode was 0.438 V, a little higher than that of the cell with air cathode, 0.430 V. The cell potential difference is due to the cathode potential difference, which can be calculated by Nernst equation (Liu, et al., 2004):

$$E_c = 1.2288 + 0.0148 \log p_{O_2} - 0.05915 pH \tag{4.2}$$

Assuming a partial pressure of oxygen in air of p=0.2 atm, the cathode potential difference for air and oxygen are 10 mV. This agrees with the cell potential difference using air or oxygen in Figure 4.6. The maximum power density of 0.126 mW/cm^2 was obtained using oxygen and the short circuit current densities were 1.78 mA/cm^2 for oxygen cathode and 0.72 mA/cm^2 for the air-breathing cathode.

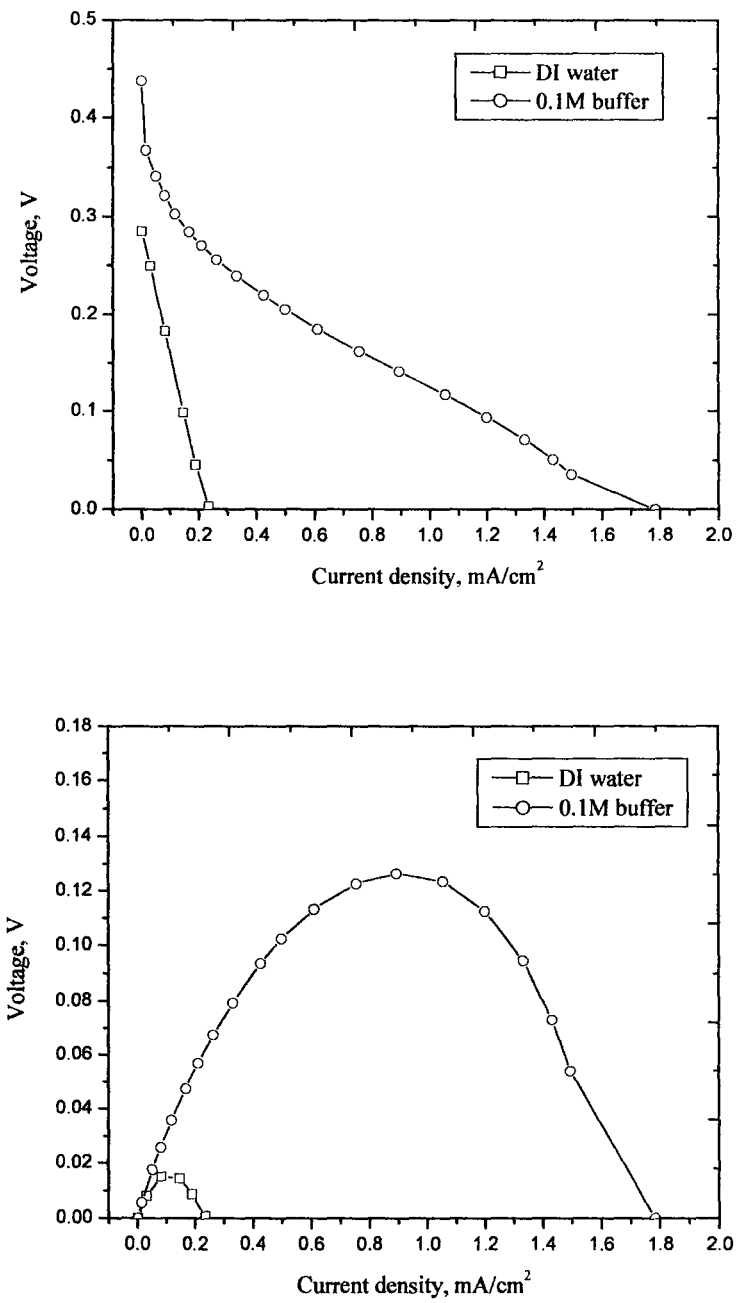

Figure 4.4 Current–voltage behavior and power density of the biofuel cell at different external loads with DI water or phosphate buffer as anolyte

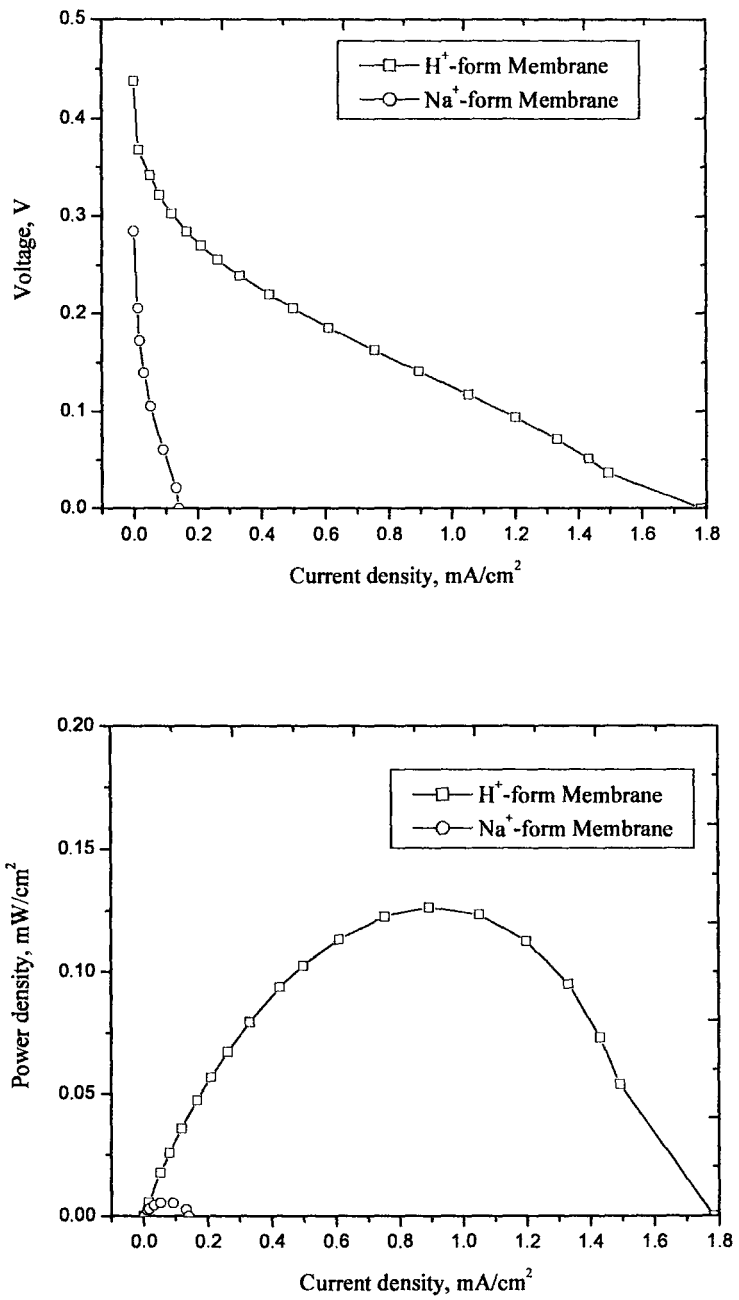

Figure 4.5 Current–voltage behavior and power density of the biofuel cell at different external loads with different form membrane

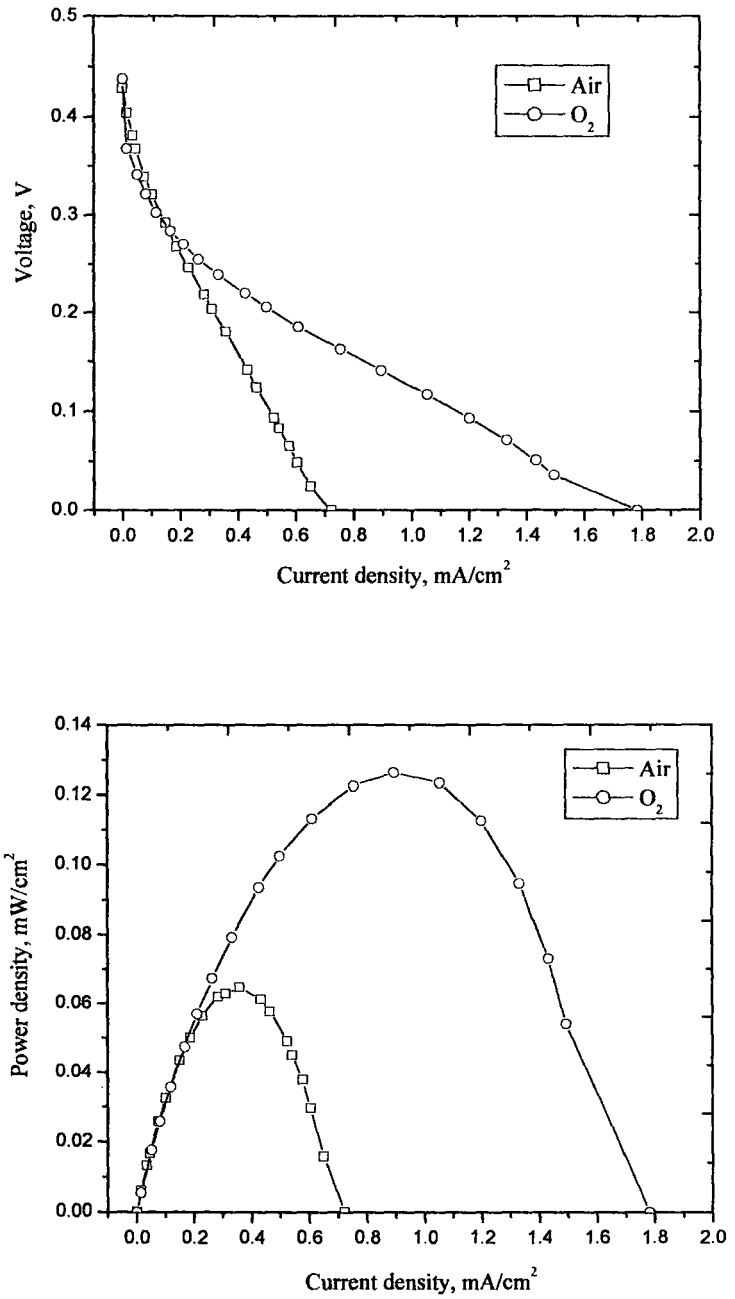

Figure 4.6 Current–voltage behavior and power density of the biofuel cell at different external loads with air/oxygen

For an air-breathing hydrogen PEM fuel cell, the maximum current density could reach 800 mA/cm^2 (Fabian et al., 2006). Oxygen supply, whether from air or pure oxygen should not limit the cell performance. Figure 4.6 seems to prove there was no concentration loss in the biofuel cell according to the IV curve shape. Therefore, limited oxygen supply from air increased other overpotentials at the cathode.

From above results, a preliminary summary is given as follows:

1) The OCP, maximum current density and power density of the biofuel cell were 0.361~0.528 V, 0.951~1.780 mA/cm^2 and 0.057~0.126 mW/cm^2, respectively, when the biofuel cell was operating with 1 g GOx, 4 mM FMCA and 200 mM glucose in 0.1 M phosphate buffer at anode chamber, a H^+-form membrane and 10 ml/min oxygen supply rate at 25°C. Its maximum power density is higher than that of a glucose/oxygen biofuel cell, 0.058 mW/cm^2, reported by Tsujimubra et al. (2002).

2) It is hard to explain that the effects of glucose concentration on the cell performance. Moreover, the cell performance seems also related to the cathode side from Figure 4.6, which is unexpected, since the purpose of using platinum-based gas diffusion cathode is to exclude the cathode's influence.

3) The results were hardly reproducible; although we tried to do everything following the correct procedure at every step, including graphite electrode cleaning, glucose and FMCA preparation, even the installation of the cell. There must be something we missed.

Therefore, anode and cathode potentials were studied separately by a reference electrode in the following experiment. In the mean time, a pH meter was used to monitor pH value changes in the anode chamber.

4.2 Effects of Glucose Concentration on the Cell IV Curve and Electrode Overpotentials

Figure 4.7 shows the effects of glucose concentration on the cell IV curve and anode and cathode overpotentials. When glucose concentration increased from 3 mM to 200 mM, the performance of the biofuel cell first increased, and then decreased.

It was discovered by surprise that the cathode had a large overpotential. As is well known, a PEM cathode can supply over 1 A/cm^2 current density. It should have a much faster reaction rate than the bio-anode. The cathode should have negligible overpotential when the cell is operating at much lower current density (around 1 mA/cm^2) according to Tafel law (Larminie and Dicks, 2003). In contrast, the cathode overpotential was larger than that of the anode, and it increased continuously with glucose concentration.

The pH value of the anolyte did not show much variation with glucose concentration. The anode overpotential decreased with glucose concentration initially. When the glucose concentration reached 67 mM, the anode overpotential no longer decreased, following saturation kinetics (Liu and Logan, 2003).

From the anode and cathode polarization curves in Figure 4.7, a good explanation can be given why the cell performance has this kind of trend with glucose concentration. Glucose concentration should have no influence on the cathode potential. The increase of cathode overpotential might be related to degradation over time evolution.

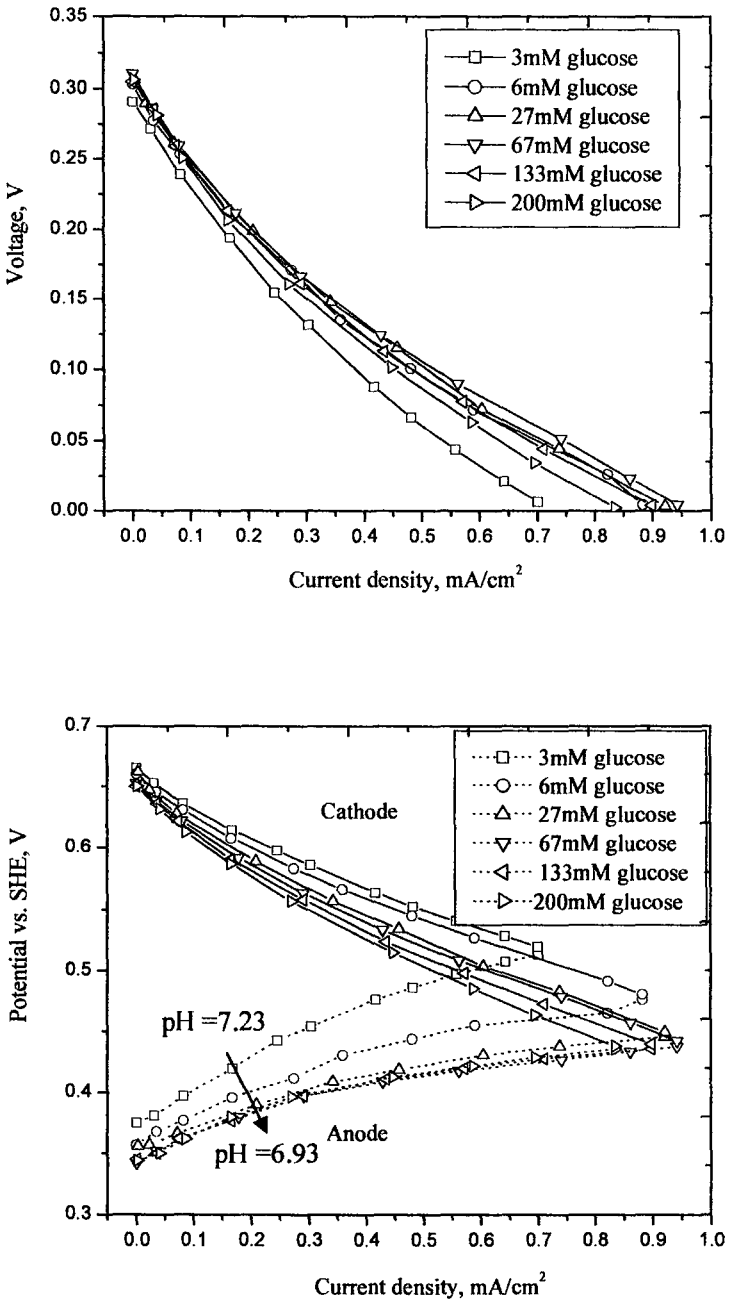

Figure 4.7 Effects of glucose concentration on the cell IV curve and anode and cathode overpotentials

4.3 Effect of Time on the Cell IV Curve and Electrode Overpotenrials

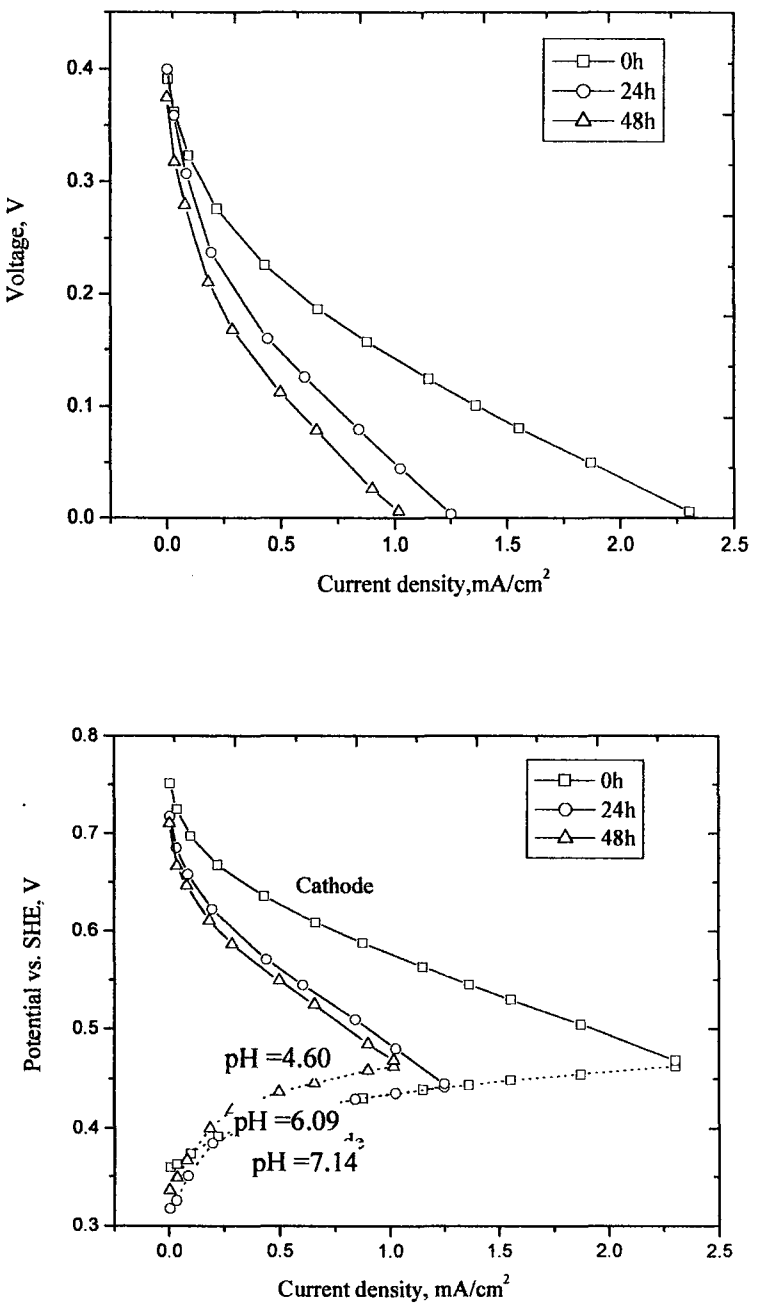

Figure 4.8 Effect of time on the cell IV curve, anode pH value and anode and cathode overpotentials

As shown in Figure 4.8, the performance of the cell decreased with time, which was mainly due to the cathode overpotential increase. In the mean time, the pH value of anolyte decreased from initial 7.23 to 4.60 after 48h. The anode overpotential did not change at pH7.23 and 6.09. When the pH value decreased to 4.60, the anode overpotential increased. This is because GOx loses its activity when pH value is less 5 or greater than 7 (Figure 1.2). The increase of pH value of anolyte shows that H^+ transport through the membrane was slower than its production rate in the anolyte (Gil, et al., 2003). It is well known that Nafion is highly conductive to H^+. The reported area resistances for Nafion 117 are in the range 0.09 to 0.35Ωcm^2 for H^+ (Rozendal et al., 2006). Why is the H^+ transport hindered in the membrane?

Figure 4.9 shows the impedance measurement results for the biofuel cell at different time. Conventionally, the resistance at the high-frequency intercept is considered to be the electrolyte resistance. Therefore, the electrolyte resistance was 1.07Ω (0.71Ωcm^2) initially, 1.21Ω (0.80Ωcm^2) after 24h and 1.25Ω (0.83Ωcm^2) after 48h. According to the structure of the biofuel cell in Figure 3.1, the electrolyte resistance is mainly from Nafion. The area resistance for Nafion from our results was greater than the reported data (Rozendal et al., 2006). Moreover, it changed with time. Nafion is a highly conductive ionic conductor, not only for H^+, but also other cations. The area resistances for Nafion 117 are 1.5 Ωcm^2 for other cations in general (Rozendal et al., 2006). Our results were exactly between the resistances for H^+ and other cations. This indicates that there should be other cations in the membrane. Except for H^+, the only cation in the anolyte is Na^+. It is thought Na^+ leads to the increase of membrane resistance. Besides, the question rises whether or not Na^+ causes the increase of the cathode overpotential?

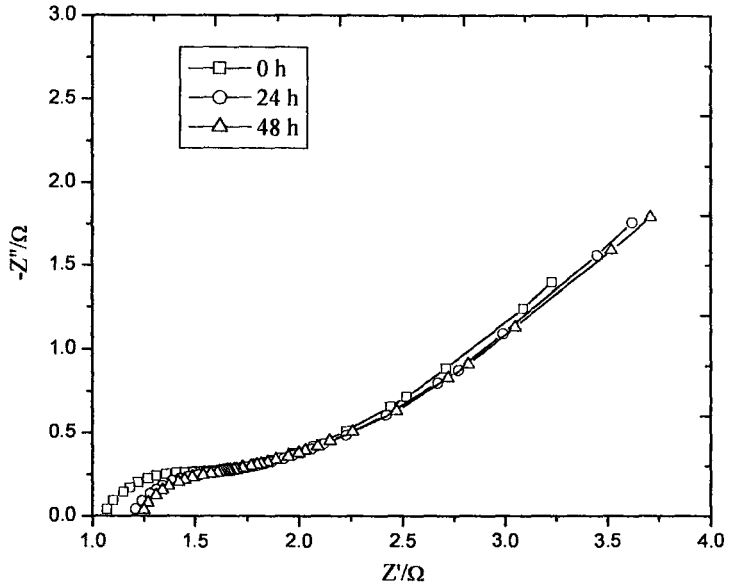

Figure 4.9 Effect of time on cell impedance

4.4 Na^+ in Membrane

To verify our suspicion, H^+-form and Na^+-form membranes were used in the biofuel cell for comparison. As shown in Figure 4.5, the biofuel cell with Na^+-form membrane had a poorer performance in comparison with the cell with H^+-form membranes. Moreover, the decrease of the cell performance was almost all due to the increase of the cathode overpotential (Figure 4.10).

Impedance measurement results are shown in Figure 4.11. It was found that Na^+-form membrane had a resistance of 1.29 Ω, which was greater than the resistance of H^+-form membrane (1.07 Ω). The reason why the resistance of H^+-form membrane is greater than the reported data (Rozendal et al., 2006) is because Na^+ has entered into the membrane once the sodium phosphate buffer is added in the anode chamber. The H^+-form membrane is not a pure H^+-form membrane, but an H^+-rich membrane.

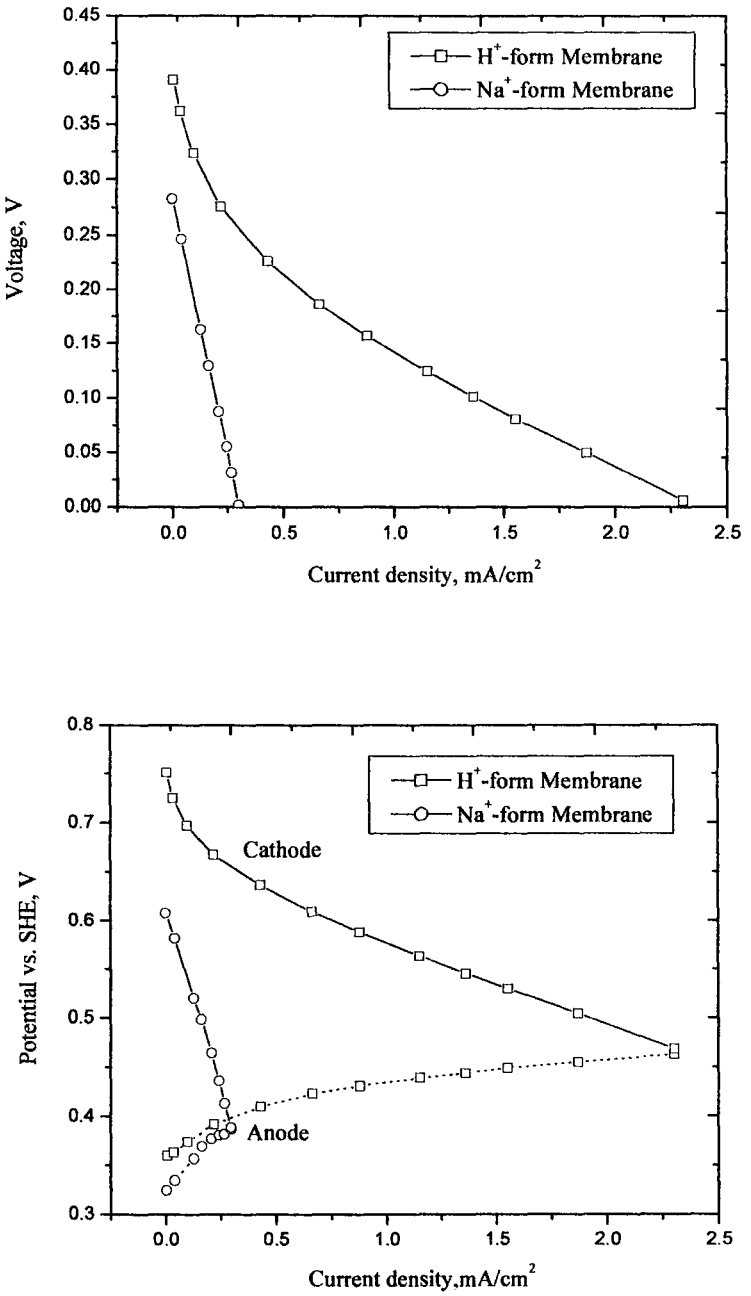

Figure 4.10 Effects of H^+-form and Na^+-form membrane on the cell IV curve and anode and cathode overpotentials

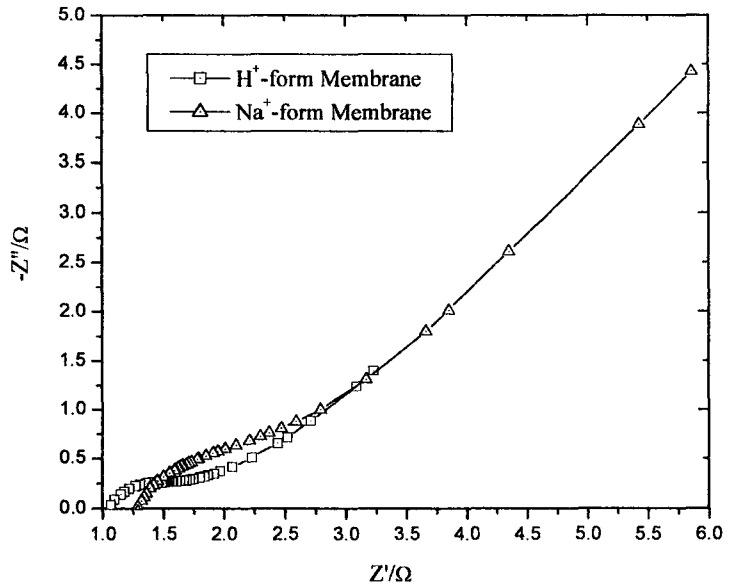

Figure 4.11 Nyquist plots of impedance spectra of the biofuel cell with an H^+-form or Na^+-form membrane

The impedance measurement results in Figure 4.11 were composed of a high frequency distorted semicircle and a low frequency linear spike. It is hard to fit the data due to the limited information from those results. However, it is believed that the high frequency semicircle should be related to electron transfer resistance. As shown in Figure 4.11, that electron transfer resistance increased when there was Na^+ in the membrane.

4.5 Na^+ in Catholyte

To confirm it was the Na^+ that caused the increase of the cathode overpotential, DI water and 0.1M NaCl were added in the cathode chamber, respectively. It was found that Na^+ caused the increase of the cathode overpotential, and thus the decrease of the cell performance, as shown in Figure 4.12.

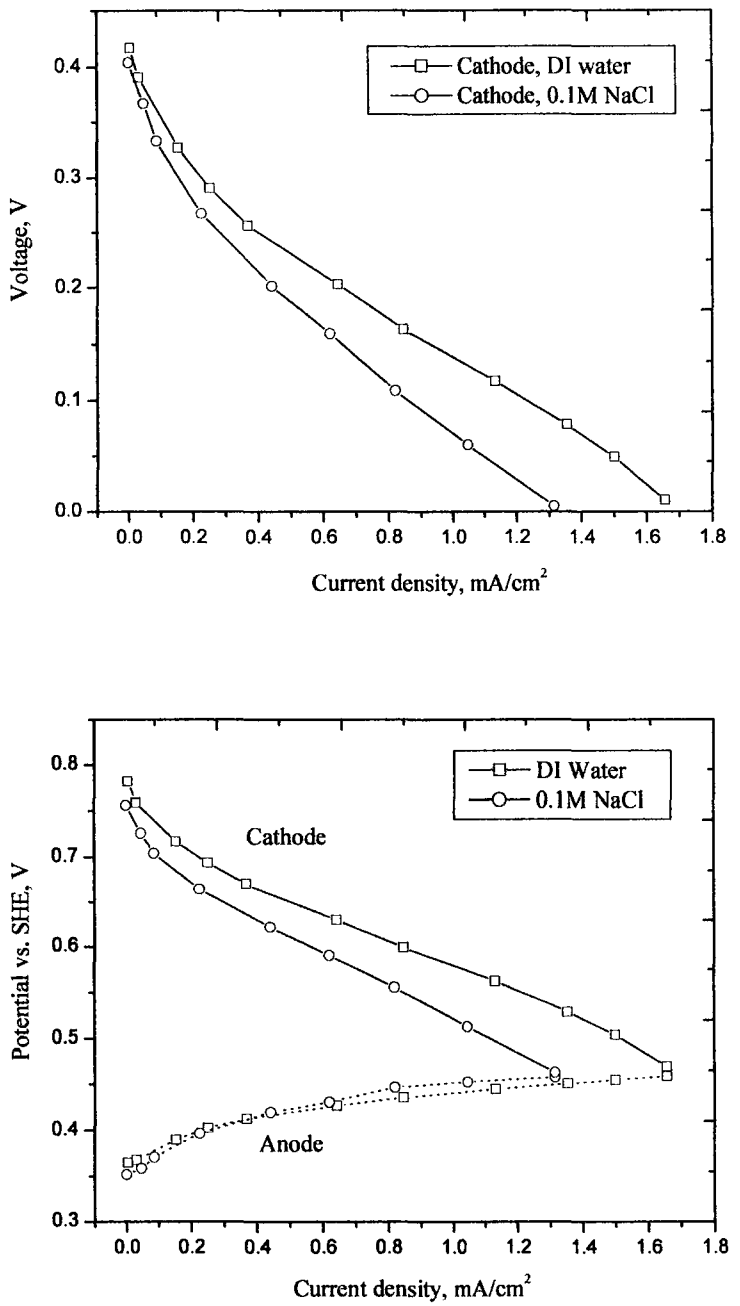

Figure 4.12 Effects of Na^+ in the catholyte on the cell IV curve and anode and cathode overpotentials

4.6 Discussion about the Role of Na^+ in the Biofuel Cell

Figure 4.13 shows a schematic diagram of H^+-form membrane in the biofuel cell with a sodium buffer. After H^+-form membrane is installed in the cell and sodium phosphate buffer is added in the anode chamber, H^+ in the membrane will be exchanged with Na^+ in the anolyte, whether at open circuit or closed circuit. Na^+ will gradually replace H^+ in the membrane and occupy all the sulfonate groups in the membrane.

As mentioned above, Na^+ in the membrane hindered H^+ transport and caused the increase of the cathode overpotential. To understand the mechanisms of that, a detailed discussion is given as follows.

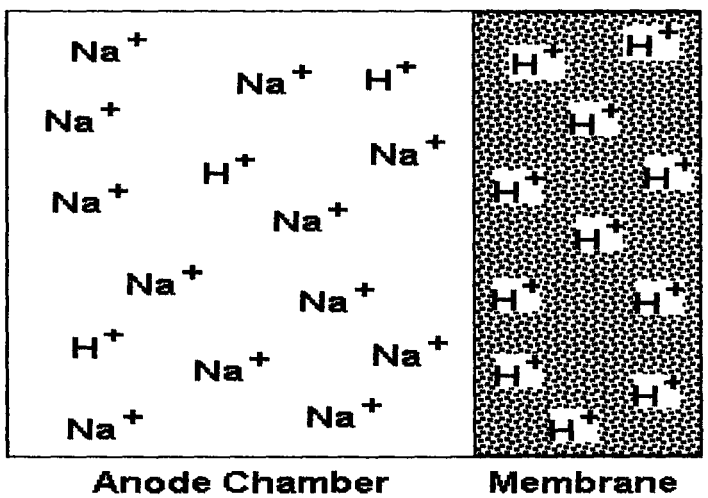

Figure 4.13 Schematic of Na^+ and H^+ concentration in the biofuel cell

4.6.1 Na^+ in Membrane

The Na^+ in the membrane has a couple of negative effects on the biofuel cell:

1) Na^+ hinders H^+ transport in the membrane;

Figure 4.8 shows H^+ transport through the membrane was slower than its

production rate in the anode chamber, especially after the cell was running for a certain time. Okada et al. (1998) studied the relationships between the membrane composition and H^+ transference number in Nafion 117. H^+ transport through the membrane markedly decreases when the amount of Na^+ occupy over 50% of the sulfonate groups (Figure 4. 14).

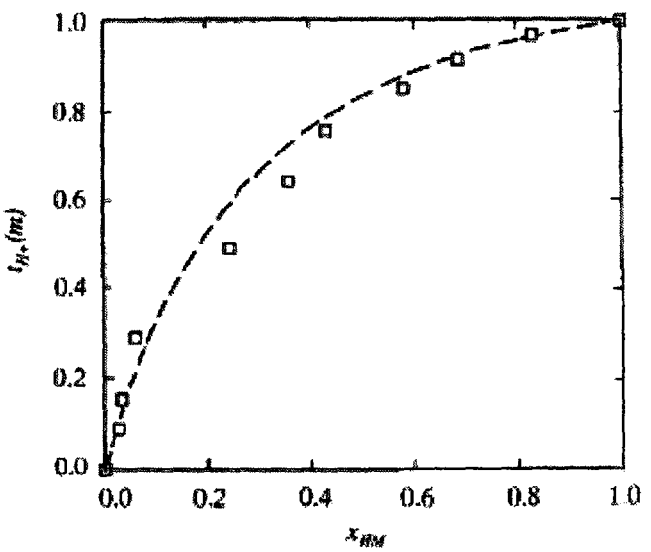

Figure 4.14 H^+ transference number in Nafion 117, t_{H+} (m) vs. membrane composition x_{HM} (Okada et al., 1998)

H^+ transport limitations in Na^+ contained Nafion also provide a new explanation for the degradation of biofuel cells. Figure 4.15 shows the cell degradation during 12 h operation. The power density decreased by 50% after 2.35 h of the cell operation. Conventionally, the decrease in the cell power output originates from the depletion of the fuel substrate, inter-penetration of the fuel and oxidizer into the respective counter compartments and the degradation of the biocatalysts (Willner et al., 1998). However, this

decrease in our biofuel cell was mainly due to H^+ transport limitations in the membrane (Figure 4.8).

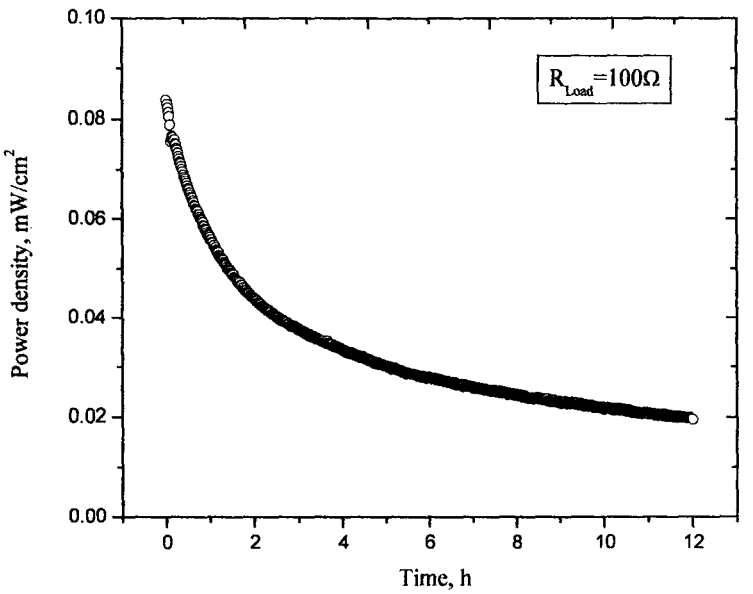

Figure 4.15 Stability of the biofuel cell power operating at external load of 100Ω as a function of time

2) Na^+ causes the increase of cathode overpotential;

Figure 4.8 also shows the cathode overpotential increased continuously with time, because more and more H^+ in the membrane was exchanged by Na^+. Figure 4.9 shows that when all of cations in the membrane became Na^+, the cathode overpotential increased more than 143 mV in comparison with H-form membrane. Rozendal et al. (2006) thought the cathode overpotential increase was due to pH value increase according to Nernst equation Eq. 4.2. Indeed, Figure 4.8 shows the cathode OCP decreased. However, the overpotential of the cathode increased more evidently when the cell was operating. Okada et al. (2001) discovered Na^+ hindered enormously the rate of charge-transfer step at

platinum covered with ionomer even with 0.1% level of Na^+. Our impedance measurement results also show electron transfer resistance increased when there is more Na^+ in the membrane (Figure 4.11).

Na^+ in the membrane hinders H^+ transport in the membrane, thus limited H^+ transport causes the increase of the cathode overpotential. The rate-limiting step in our biofuel cell is H^+ transport, not at cathode. Therefore, the conventionally believed relationship between rate-limiting step and overpotential described in 2.3 needs to be revised.

One question which needs more attention is why the cathode has considerably large overpotential initially. The reason is that when sodium phosphate buffer is added in the cell, H^+ in the membrane will be immediately exchanged with Na^+ in the anolyte. When we start to do measurements, there has been some Na^+ in the membrane, which causes the increase of the cathode overpotential.

4.6.2 Na^+ at Cathode

When an H^+-form membrane is completely transformed to a Na^+-form membrane, H^+ transference number is zero (Figure 4.14). Therefore, H^+ can not be transported through the membrane, and Na^+ is responsible for the transport of cations through the membrane, which is consistent with the claims of Rozendal et al. (2006). When H^+ is not transported to cathode, what is the reaction, which happens at the cathode?

It is obvious that the reduction of Na^+ at the cathode is impossible, due to its low reduction potential (Brett et al., 1993):

$$Na^+ + e^- \rightarrow Na; E_0 = -2.71V \tag{4.3}$$

Rozendal et al. (2006) thought the oxygen reduction consumed H^+ from the basic catholyte in their cell equimolarly with electrons at the cathode, as shown in Eq. 1.2, and Na^+ was transported from anolyte through the membrane to the catholyte to keep electroneutrality on the cathode side. However, this claim contradicts Yeager's point of view (1984). He thought oxygen reduction was considered to proceed by the following two overall pathways, depending on in alkaline solutions or acid solutions:

Alkaline solutions: $O_2 + 2H_2O + 4e^- \rightarrow 4OH^-; E_0 = 0.401V$ (4.4)

Acid solutions: $O_2 + 4H^+ + 4e^- \rightarrow 2H_2O; E_0 = 1.229V$ (4.5)

Free energy relationships for the reduction of oxygen in acid and basic solution at 25°C were given in Figure 4.16 and 4.17 by Tarasevich et al. (1983). Therefore, the oxygen reduction at the cathode with basic catholyte in the biofuel cell should proceed following Eq. 4.4.

Although the Nernst equations for the reaction of Eq.4.4 and Eq. 4.5 are the same as Eq. 4.2, one difference between Eq. 4.4 and Eq. 4.5 is H^+-involved in Eq. 4.5. For the gas diffusion cathodes in our biofuel cell and Liu and Logan's microbial fuel cell (2004), when the H^+ transport is blocked, there is no H^+ available to take part in the reaction in Eq. 4.5. It means the oxygen reduction at the cathode under this condition can only follow Eq. 4.4.

Another difference between Eq. 4.4 and Eq. 4.5 is the production of water in Eq. 4.5 and the consumption of water in Eq. 4.4. If the oxygen is reduced following Eq. 4.4, where does the water come from?

Water can be obtained from air or oxygen at the cathode, but a mount of water from this source is negligible. A more important channel is the water transported with Na^+

from anolyte. Figure 4.18 shows the water transfer number in Nafion 115 plotted as a function of membrane composition x_{HM}. The water transfer number was 2.5 and 9.2 for H^+ form and Na^+ form in Nafion 115, respectively (Okada et al., 1998).

Na^+ will deposit at the gas diffusion cathode after it is transported from the anolyte in our biofuel cell. It was observed that when Cu wire was used at the cathode sometimes, the color of the Cu wire was changed from bright copper-color to gray, whereas it did not change in phosphate buffer or Tris buffer with GOx, Glucose, and FMCA. It was verified that the color of Cu wire indeed changed in the NaOH solution. The second piece of evidence is when the graphite current collector at the cathode side was cleaned sometimes, the cell performance increased greatly. That is why it was hard to obtain reproducible data in the previous experiments.

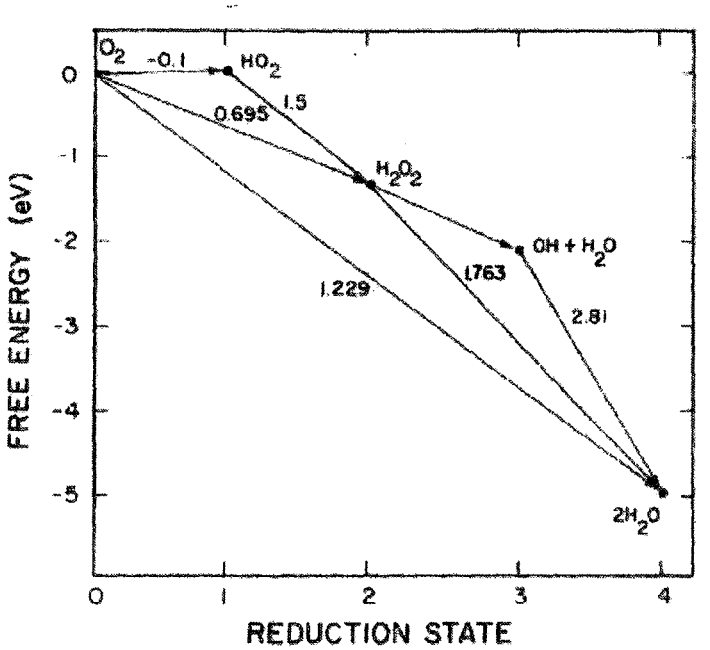

Figure 4.16 Free energy relationships for the reduction of oxygen in acid solution at 25°C (Tarasevich et al., 1983)

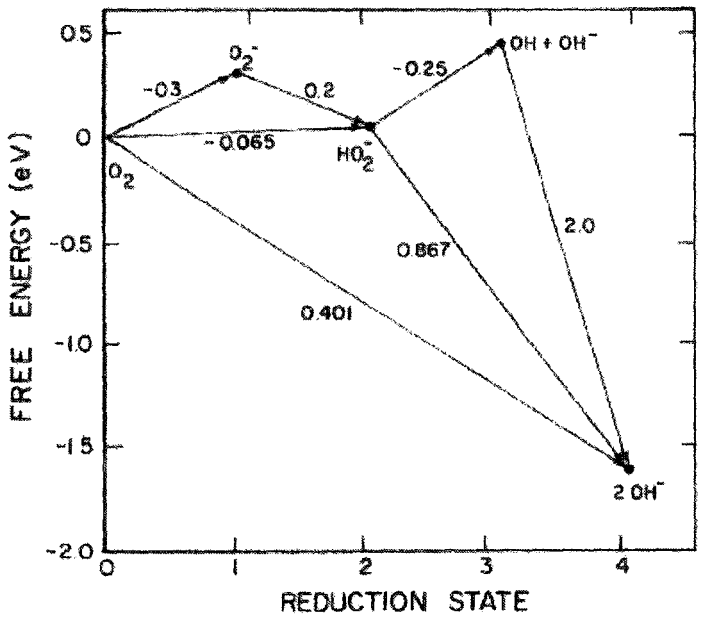

Figure 4.17 Free energy relationships for the reduction of oxygen in basic solution at 25°C (Tarasevich et al., 1983)

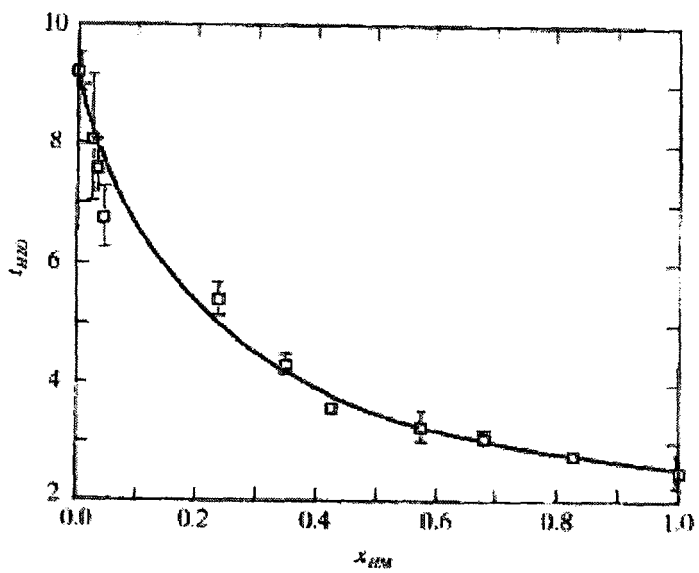

Figure 4.18 Water transfer number in Nafion 115 plotted as a function of membrane composition x_{HM} (Okada et al., 1998)

In conclusion, a complete understanding of the operating process of our biofuel cell is as follows. Initially, H^+ is mainly transported from the anolyte through the membrane to the cathode. In the mean time, Na^+ in the anolyte exchanges with H^+ in the membrane. As time goes on, more and more Na^+ occupies the sulfonate groups in the membrane. As a result, H^+ transport in the membrane is hindered, which leads to the pH value of the anolyte decreases, the cathode overpotential increases and the cell performance decreases. When Na^+ occupies all of sulfonate groups in the membrane, only the Na^+ from the anolyte can pass through the membrane. The oxygen reacts with the water transported with Na^+ and electrons from the external circuit to produce OH^-, which balances with the transported Na^+ to keep electroneutrality at the cathode. The cell is no more a biofuel cell involving H^+ at that time.

4.7 Effect of Tris Buffer on the Cell IV Curve and Electrode Overpotentials

As alkali and alkaline earth metal cations or transitional metal cations show the tendency to suppress the kinetics of oxygen reduction reaction at the platinum-Nafion interface (Okada, et al, 2001), an alternative is to choose a kind of buffer without these kinds of cations for the biofuel cell.

$TrisH^+$/Tris buffer is a very common biological buffer, which does not have the above mentioned cations (Figure 4.19). Figure 4.20 shows the effects of DI water, 0.1M Tris buffer and 0.1M sodium phosphate buffer as anolyte, respectively on the cell performance and anode and cathode potentials. The highest performance was obtained from the experiment which employed sodium phosphate buffer followed by Tris buffer. As shown in Figure 4.4, the lowest performance was obtained from the cell with DI water as anolyte. The anode and cathode overpotentials were all increased for the cell with DI water and Tris buffer as anolyte in comparison with that with phosphate buffer as anolyte.

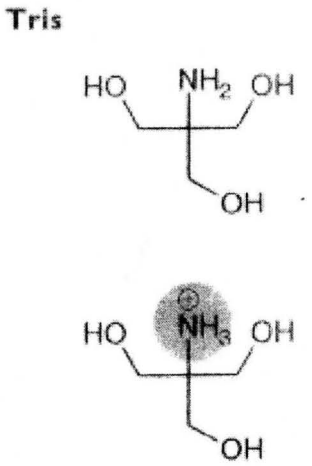

Figure 4.19 Schematic of TrisH+/Tris buffer (Beynon and Easterby, 1996)

pH value did not show much variation for the phosphate buffer anolyte (from 7.23 to 7.05), whereas pH changes was from 7.42 to 4.45 for the Tris buffer anolyte after one IV curve measurement. pH value changes of DI water anolyte were not obtained due to its lower ionic strength. The solubility of FMCA in sodium phosphate buffer is around 4mM followed by Tris buffer (2mM). FMCA hardly dissolves in DI water. Therefore, the increase of anode overpotential is due to the increase of electron transfer resistance and the decrease of pH value of anolyte, whereas the increase of cathode overpotential is due to the limited H^+ transport, caused by the decreased driving force for H^+ transport and the presence of Tris ions in the membrane. The Tris buffer does not constitute a solution to the problem. To improve the cell output, a kind of buffer, which has no Na^+ or other cations, which limit H^+ transport in the membrane, a good ability to resist pH change, and a good solubility for mediators, is necessary.

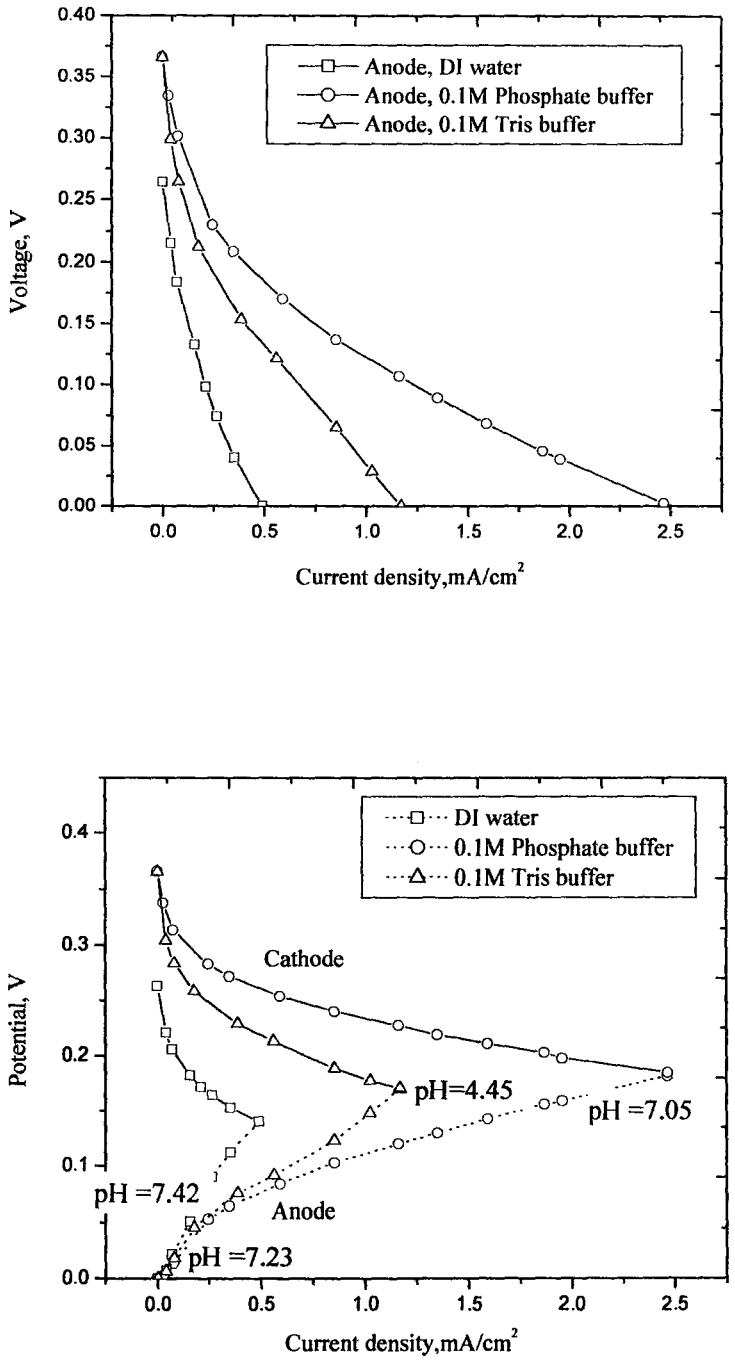

Figure 4.20 Effect of anolyte on the cell IV curve and electrode overpotentials

Chapter 5 Conclusions

In this thesis, the rate-limiting step is determined in a biofuel cell with a bio-anode, a Nafion membrane and a conventional, platinum-based cathode using reference electrode and EIS methods. It was discovered by surprise that the cathode overpotential dominated the cell overpotential. Na^+ in the membrane was found to hinder H^+ transport. The cathode overpotential increased due to the presence of Na^+ in the membrane and at the cathode. The limited H^+ transport causes the increase of the cathode overpotential. H^+ transport is the rate-limiting step in our biofuel cell, rather than commonly believed electron transport. The conventionally believed relationship between rate-limiting step and overpotential needs to be revised. Moreover, the cell power output degradation is not due to the conventionally believed depletion of the fuel substrate, inter-penetration of the fuel and oxidizer and the degradation of the biocatalysts, but the limited H^+ transport.

The existing oxygen reduction mechanism at the cathode was questioned and revised. A complete description of the operating process of our biofuel cell was presented. Initially, mainly H^+ is transported from the anolyte through the membrane to the cathode. In the mean time, Na^+ in the anolyte exchanges with H^+ in the membrane. As time goes on, more and more Na^+ occupies the sulfonate groups in the membrane. As a result, H^+ transport in the membrane is hindered, which leads to the pH value of the anolyte decreases, the cathode overpotential increases and the cell performance decreases. When Na^+ occupies all of sulfonate groups in the membrane, only the Na^+ from the anolyte can pass through the membrane. The oxygen reacts with the water transported with Na^+ and electrons from the external circuit to produce OH^-, which balances with the transported

Na^+ to keep electroneutrality at the cathode. The cell is no more a biofuel cell involving H^+ at that time.

Tris buffer without Na^+ was utilized as alternative anolyte in the biofuel cell. It was found that the cell with Tris buffer had a poorer performance in comparison with sodium phosphate buffer due to the increases of the anode and cathode overpotentials. Tris buffer does not constitute a solution to the problem.

This work represents a step toward a more complete understanding of the properties of biofuel cells. Guided by a better understanding of the performance limiting factors in biofuel cells, multiple changes in the design and operation conditions of biofuel cells, such as the application of OH^- exchange membrane in bioufel cells, can be considered.

References

Aelterman, P., Rabaey, K., Pham, H.T., Boon, N., Verstraete, W. (2006) *Environ. Sci. Technol.*, **40**(10), 3388

Alberty, R.A. (2000) *Biochemical Education*, **28**, 12

Alferov, S.V., Tomashevskaya, L.G., Ponamoreva, O. N., Bogdanovskaya, V.A., Reshetilov, A.N. (2006) *Russian Journal of Electrochemistry*, **42**(4), 403

Amphelett, J.C., Baumert, R.M., *Ma*nn, R.F., Peppley, B.A., Roberge, P.R. (1995) *J.Electrochem. Soc.* **142**(1), 1

Ayato Y., Kunimatsu K., Osawa M., Okadaa, T. (2006) *Journal of The Electrochemical Society* **153**(2), A203

Barsoukov, E., Macdonald, J.R. (2005) *Impedance Spectroscopy*, John Wiley and Sons Ltd., Hoboken, New Jersey; 2nd ed.

Barton, S.C., (2005) *Electrochimica Acta* **50**, 2145

Barton, S.C., Gallaway J., Atanassov, P. (2004) *Chem. Rev.* **104**, 4867

Beynon, R.J., Easterby, J.S. (1996) *Buffer Solutions: The Basics*, Oxford University Press, Oxford, New York

Brett, C.M.A., Brett, A.M.O (1993) *Electrochemistry : principles, methods, and applications,* Oxford University Press, Oxford, New York

Bullen, R.A., Arnot T.C., Lakeman J.B., F.C. Walsh (2006) *Biosensors and Bioeletronics* **21**, 2015

Chaudhuri, S. K., Lovely, D. R. (2003) *Nature Biotechnol.* **21**, 1229

Choban, E.R., Waszczuk, P., Kenis, J.A. (2005) *Electrochemical and Solid-State Letter* **8**, (7) A348

Fabian, T., Posner, J.D., O'Hayre, R., Chac, S., Eaton, J.K., Prinz, F.B., Santiago, J.G. (2006) *Journal of Power Sources*, **161**, 168

Garcia, S.L. (2001) MASc Thesis, Toronto University

Gasteiger, H.A., Panels, J.E., Yan S.G. (2004) *Journal of Power Source* **127**,162

Gil, G.C., Chang, I.S., Kim B.H., Kim, M., Jang, J.K., Park, H.S., Kim, H.J., (2003) *Biosensors and Bioelectronics*, **18**, 327

Han, J.N., Park, G.G., Yoon, Y.G., Yang, T.H., Lee, W.Y., Kim, C.S. (2003) *International Journal of Hydrogen Energy* **28**, 609

Haselkorn, A. (2002) *Daily Californian*, Berkeley, California, 28 August

Heller, A. (2004) *Phys. Chem. Chem. Phys.* **6**, 209

He, Z., Minteer, S.D., Angenent, L.A.T. (2005) *Environ. Sci. Technol.*, **39**, 5262

He, Z., Wagner, N., Minteer, S.D., Angenent, L.T. (2006) *Environ. Sci. Technol.*, **40**, 5212

He, W., Nguyen, T.V. (2004) *J. Electrochem. Soc.* **151,** A185

Jaouen, F., Lindbergh, G., Wiezell, K., (2003) *Journal of The Electrochemical Society*, (**150)** A1711

Jon Scaife, J., Dove, C. (2000) *Phys. Educ.* **35**(5), 343

Katz, E., Shipway, A.N., Willner, I.(2003) *Handbook of Fuel Cells-Fundamentals, Technology and Applications*, Vielstich, W., Gasteiger, H.A., Lamm, A., Eds.; John Wiley and Sons, Ltd. London,; Vol.1, 355

Katz, E., Willner, I., Kotlyar A.B. (1999) *J. Electroanal. Chem.* **479**, 64

Karyakin, A.A, Morozov S.V., Karyakina E.E, Varfolomeyev S.D., Zorin N.A., Cosnier S. (2002) *Electrochemistry Communications* **4**, 417

Kim, J., Jia, H., Wang P. (2006) *Biotechnology Advances* **24**, 296

Larminie, J., Dicks, A. (2003) *Fuel Cell Systems Explained*, John Wiley and Sons Ltd., West Sussex, England; 2nd ed.

Lee, C.G., Nakano, H., Nishina, T., Uchida, I., Kuroe, S.(1998) *J.Electrochem. Soc.*, **145**, 2747

Liu, H., Logan, B.E. (2004) *Environ. Sci. Technol.* **38**, 4040

Liu, H., Ramnarayanan, R., Logan, B.E. (2004) *Environ. Sci. Technol.* **38**, 2281

Liu, Y., Wang, M., Zhao, F., Liu, B., Dong, S. (2005) *Chem. Eur. J.* **11**, 4970

Mano, N., Mao, F., Heller, A. (2002) *JASC,* **124,** 12962

Marcus, R.A. (1993) *Rev. Mod. Phys.* **65,** 599

Okada, T., Ayato, Y., Satou, H., Yuasa, M., Sekine, I. (2001) *J.Phys.Chem.B.* **105,** 6980

Okada, T., MØller-Holst, S., Gorseth, O., Kjelstrup, S. (1998) *Journal of Electroanalytical Chemistry*, **442,** 137

Palmore, G.T.R., Whitesides, G.M. (1994) *ACS Symp. Ser.*, **566**, 271

Persson, B., Gorton, L., Johansson, G., Torstensson, A. (1985) *Enzyme Microb. Technol.*7, 549

Rabaey, K., Boon, N., Hofte, M., Verstraete, W. (2005) *Environ. Sci. Technol.* **39**, 3401

Rabaey, K., Lissens, G., Siciliano, S.D., Verstraete, W. (2003) *Biotechnology Letters* **25**, 1531

Rozendal, R., Hamelers, H.V.M., Buisman C.J.N., (2006) *Environ. Sci. Technol.* **40**, 5206

Rabaey, K. & Verstraete, W. (2005) *Trends in Biotechnology* **23**, 291

Shukla, A.K., Suresh, P., Berchmans, S. & Rajendran, A. (2004) *Current Science* **87**, 455

Strathmann, H. (2004) *Ion-exchange Membrane Separation Processes.* Amsterdam, Boston, Elsevier

Tamaki, T., Yamaguchi, T. (2006) *Ind. Eng. Chem. Res.* **45**, 3050

Tarasevich, M., Sadkowski, A., Yeager, E., *Comprehensive Treatise of Electrochemistry* (1983) Edited by Conway, B., Bockris, J., Yeager, E., Khan, S., White, R., Plenum Press, New York, Vol.7, 301

Thomas, S.C., Ren, X., Gottesfeld, S., Zelenay, P. (2002) *Electrochim. Acta*, **47**, 3741

Tsujimura, S., Kano, K., Ikeda, T. (2002) *Electrochemistry* **70**, 940

Wang, C. (2004) *Chem. Rev.* **104**, 4727

Wang, M., Shen, Y., Liu, Y., Wang, T., Zhao, F., Liu B., Dong, S. (2005) *Journal of Electroanalytical Chemistry*, **578**, 121

Wagner, N., Schnurnberger, W., Muller, B., Lang, M. (1998) *Electrochim. Acta*, **43**(24), 3785

Wilkinson, S. (2000) *Autonomous Robots*, **9**, 99

Willner, I., Katz, E., Patolsky, F., Bückmannb, A.F. (1998) *J. Chem. Soc., Perkin Trans.***2**, 1817

Yeager, E. (1984) *Electrochim. Acta*, **29**, 1527

Zaluski, C.S. (1997) PhD Thesis, McMaster University

Appendices

A1 Error Analysis and Explanation to the Repeatability of Experimental Results and the Cell Output without glucose

In the initial stage of our research, the experimental results were hardly reproducible, as mentioned in p52 and p61. The reasons could be associated with either the instruments or cell preparation. Current and voltage were measured by HP 3478A multimeter (Electrolab Inc., USA), using 5 1/2 Digit mode. The measurement accuracy is 0.1~1 μV for voltage measurement and 1 μA for current measurement, respectively. The open circuit voltage and the maximum current of our cell are 0.361~0.528 V and 0.627 ~ 1.175 mA, respectively. Therefore the possible error from the instrument is 0.19~0.28% for the open circuit voltage measurement, and 0.09~0.16% for the maximum current measurement, respectively. Clearly, the instrument is not the source of the poor reproducibility.

Therefore, the poor reproducibility of experimental results must be due to the cell preparation. When the cell was reassembled, the initial conditions were hardly comparable to the previous ones, even though the cell was operated under the same parameters. However, the same trend of GOx and FMCA concentration on the cell performance can be found each time (Figure 4.1 and 4.7). It was later discovered that the poor reproducibility of experimental results was due to the presence of Na^+ in the membrane and at the cathode. Not only Nafion membrane, but also the graphite current collector at the cathode, need to be treated before each experiment. Beyond that point, a good reproducibility of experimental results could be achieved, as shown in Figure 4.3 and 4.20.

Regarding the non-zero output of the cell with no glucose (Figure 4.1), one

possibility is the remnants of glucose, GOx and FMCA stuck at the porous graphite anode used in the previous measurements. The anode is cleaned with 1.0 M NaOH followed by 1.0 M HCl after each experiment and stored in distilled water before use. GOx would lose all of its activity in this strong acid and basic solution. Even though there is some glucose absorbed at the anode, glucose can not be decomposed without GOx. Therefore, the cell output without glucose is ascribed to the remnants of FMCA at the anode, which is hard to be removed completely.